

AD-A099 383

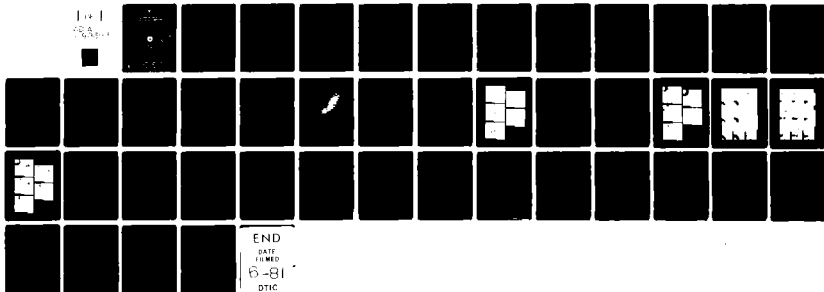
NATIONAL OCEANIC AND ATMOSPHERIC ADMINISTRATION NORM--ETC F/G 4/2
FAA RADARS AND THEIR DISPLAY OF SEVERE WEATHER (THUNDERSTORMS). (U)
JUL 80 K E WILK, J T DOOLEY DOT-FA77WAI-724

UNCLASSIFIED

FAA-RD-80-65

NL

101
FAA



Report No. FAA-RD-80-85

LEVEL II

12

5

FAA RADARS AND THEIR DISPLAY OF SEVERE WEATHER (THUNDERSTORMS)

Kenneth E. Wilk
J.T. Dooley

National Severe Storms Laboratory
Environmental Research Laboratories
National Oceanic and Atmospheric Administration

AD A099383



DTIC
ELECTE
MAY 27 1981

July 1980
Final Report

Document is available to the U.S. public through
the National Technical Information Service,
Springfield, Virginia 22161.

Prepared for

U.S. DEPARTMENT OF TRANSPORTATION
FEDERAL AVIATION ADMINISTRATION
Systems Research & Development Service
Washington, D.C. 20590

*Original contains color
plates. All DTIC reproductions
will be in black and
white.

DTIC FILE COPY

81 5 26 015

NOTICE

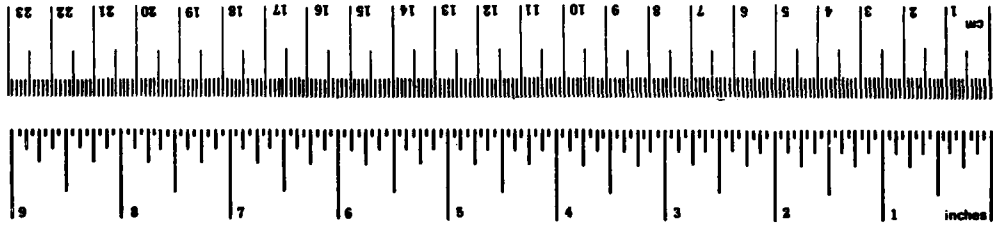
This document is disseminated under the sponsorship of the Department of Transportation in the interest of information exchange. The United States Government assumes no liability for its contents or use thereof.

Technical Report Documentation Page

1. Report No. FAA-RD-80-65		2. Government Accession No. AD-A099 383		3. Recipient's Catalog No.	
4. Title and Subtitle FAA RADARS AND THEIR DISPLAY OF SEVERE WEATHER (THUNDERSTORMS)		5. Report Date July 1980		6. Performing Organization Code	
7. Author(s) Kenneth E. Wilk and J. T. Dooley		8. Performing Organization Report No.		9. Performing Organization Name and Address National Severe Storms Laboratory Environmental Research Laboratories National Oceanic and Atmospheric Administration	
12. Sponsoring Agency Name and Address Department of Transportation Federal Aviation Administration Systems Research and Development Service Washington, D. C. 20590		10. Work Unit No. (TRAIS)		11. Contract or Grant No. DOT FA77WAI-724	
15. Supplementary Notes		13. Type of Report and Period Covered Final Report		14. Sponsoring Agency Code ARD-412/ARD-231	
16. Abstract <p>The relative performances of FAA ASR and ARSR Air Traffic Control radars are compared with the WSR-57 weather radar using simple models of time-dependent reflectivity profiles from severe thunderstorms. Results show the relatively wide vertical beams of FAA radars are helpful for early detection of new rain cells developing aloft. This better detection depends on range and is most useful within 65 n.mi. (120 km). Beyond 110 n.mi. (204 km), the FAA ARSR radars receive less returned signal and therefore underestimate storm strength more than the WSR-57, especially when the first heavy precipitation and hail have reached the ground. Because the FAA radar antennas are tilted and the beam axis is usually several degrees above the horizon, the return tends to maximize during storm development, but may decrease below severe weather indications while severe weather is occurring.</p>					
17. Key Words Severe Thunderstorms Airport Surveillance Radar Air Route Surveillance Radar			18. Distribution Statement Document is available to the public through the National Technical Information Service, Springfield, VA 22161.		
19. Security Classif. (of this report) Unclassified		20. Security Classif. (of this page) Unclassified		21. No. of Pages 42	22. Price

METRIC CONVERSION FACTORS

Approximate Conversions to Metric Measures		Approximate Conversions from Metric Measures	
When You Know	Multiply by	To Find	Symbol
LENGTH			
inches	2.5	centimeters	cm
feet	30	meters	m
yards	0.9	meters	m
miles	1.6	kilometers	km
AREA			
square inches	6.5	square centimeters	cm ²
square feet	0.09	square meters	m ²
square yards	0.8	square meters	m ²
square miles	2.6	square kilometers	km ²
acres	0.4	hectares	ha
MASS (weight)			
ounces	28	grams	g
pounds	0.45	kilograms	kg
short tons (2000 lb)	0.9	tonnes	t
VOLUME			
teaspoons	5	milliliters	ml
tablespoons	15	milliliters	ml
fluid ounces	30	milliliters	ml
cups	0.24	liters	l
pints	0.47	liters	l
quarts	0.95	liters	l
gallons	3.8	liters	l
cubic feet	0.03	cubic meters	m ³
cubic yards	0.76	cubic meters	m ³
TEMPERATURE (exact)			
Fahrenheit temperature	5/9 (after subtracting 32)	Celsius temperature	°C
TEMPERATURE (exact)			
Celsius temperature	9/5 (then add 32)	Fahrenheit temperature	°F



*1 in = 2.54 (exactly). For other exact conversions and more detailed tables, see NBS Misc. Publ. 286, Units of Weight and Measures, Price \$2.25, SD Catalog No. C13.10-286.

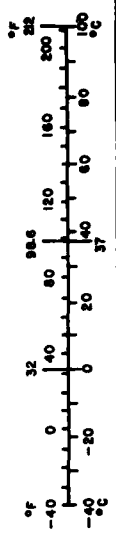


TABLE OF CONTENTS

	Page
LIST OF FIGURES AND TABLE	v
1. INTRODUCTION	1
2. PAST RESEARCH AND RELEVANT FINDINGS	3
2.1 First Echo Characteristics	6
2.2 Relation of Storm Pattern on NWS Radar Reports	10
3. EFFECT OF BEAM PATTERNS ON STORM DETECTION	10
4. SUMMARY FOR STRONG, SEVERE, AND VERY SEVERE THUNDERSTORMS	23
5. CONCLUSIONS	24
SUPPLEMENTARY REMARKS	25
ACKNOWLEDGMENTS	26
REFERENCES	26
APPENDIX A - RADAR RESPONSES TO STORM PROFILES	29
APPENDIX B - MODEL STORM PROFILE DATA	34

Accession For	
NTIS GRA&I	<input checked="" type="checkbox"/>
DTIC TAB	<input type="checkbox"/>
Unannounced	<input type="checkbox"/>
Justification	
By	
Distribution/	
Availability Codes	
Dist	Avail and/or Special
A	

LIST OF FIGURES AND TABLE

Figure	Page
1. Vertical distribution of precipitation as seen by a multiple-beam, air traffic control radar [after Pell, 1971].	5
2. Examples of vertical profiles of precipitation return and their descent with time [after Hamilton, 1966, and Dennis et al., 1970].	7
3. Frequency distributions of first echo bases, tops, and vertical growth rates observed in nonsevere storms in projects Whitetop and Metromex (Missouri) [after Johnson and Dungey, 1978].	8
4. Approximate temperatures at heights where first echoes form in nonsevere storms in Texas [after Carbone et al., 1976].	9
5. Schematic illustration of the time-height evolution of the radar echo from nonsevere storms [after Johnson and Dungey, 1978].	9
6. Composite of "snapshot" measurements of maximum echo height and surface reflectivity for 1305 observations made at five WSR-57 radar sites.	11
7. Geographical changes in the variation of echo height surface reflectivity measured with 29 NWS, WSR-57 radars for a selected one-month period in August 1965.	12
8. Precipitation growth and descent patterns used to simulate reflectivity profiles for determining effects of beam patterns of NWS and FAA radars.	12
9. Vertical reflectivity cross sections used to represent initial echo growth in storms of increasing severity.	13
10. Reflectivity data from the narrow beam (0.8 deg.) NSSL Doppler radar, showing the relatively low tops and low maximum reflectivities associated with marginally severe thunderstorm (Model 3).	14
11. (a, b, and c) Reflectivity data from the NSSL Doppler radar, showing the first development of the severe thunderstorms.	17, 18, & 19

Figure	Page
12. Profiles of mean and median reflectivity of nonsevere thunderstorms [after Konrad, 1978].	21
13. Profiles of mean core reflectivity for various categories of maximum reflectivity [after Konrad, 1978].	21
14. (a) Comparison of reflectivity in rain only and hail producing storms, and (b) Observed heights of 45 dBZ reflectivity levels in rain only and hail producing storms.	21
15. Reflectivity profiles which depict the performance of the WSR-57, ASR-8, and ARSR-1L radars at various ranges given model 1 storm profile at time 30 (when heavy rain has reached the ground).	22
Table 1. Comparative Radar Beam Characteristics	2

FAA RADARS AND THEIR DISPLAY OF SEVERE WEATHER (THUNDERSTORMS)

1. INTRODUCTION

In the Phase I National Severe Storms Laboratory (NSSL) report on this investigation of severe weather portrayal on FAA Air Traffic Control (ATC) radars, Zittel [1978] summarized some causes of severe thunderstorms and explained, logically, several shapes and patterns characteristic of their radar echoes. Since precipitation is carried by (and therefore traces) the airflow in and beneath storm clouds, the shapes of radar echoes relate mainly to the configuration of rising and descending currents. The configurations of echoes from severe storms change with time as the drafts become laterally separated, and ascending cyclonic (counter-clockwise) circulations become organized. This organization encourages the regenerative precipitation process within the storm; while rate of rise and fall of air (again, within the storm) controls conversion of cloud moisture to rain, and affects suspension and growth of hail aloft. The stability and duration of the radar echo are intrinsic to these processes.

Because radar return is substantially from raindrops (average diameter about 2 mm), shape and intensity of echo on air traffic controllers' PPI scopes reflect the three-dimensional distribution of rain occurring everywhere within the radar beam. Also, since present day operational radars do not "see" wind and air flow patterns directly, controllers must infer the presence of turbulence, strong outflow gusts, and tornadoes from reflectivity structure, and must envision rain configured in response to organized flow within the storm. By experience we have learned that when organized storms persist, sharp boundaries develop between rain-cooled air in the downdraft and warm moist air in the updraft--boundaries which become local line squalls with strong gusts, heavy rain and severe turbulence. If cyclonic rotation develops within the cloud, then along these boundaries, tornadoes also are possible.

In summary, the problem forecasters and controllers must face in interpretation of radar displays of severe storms is early recognition of echo patterns which signal that specific conditions are developing within the storm cloud. This report considers unique distributions of rain and hail within severe thunderstorms and the probable effect on echo intensities seen on FAA ATC radars and National Weather Service weather radars. Table 1 lists the comparative radar beam characteristics of the FAA and NWS radars considered applicable to the discussions in this report. As in Zittel's report, it is expected that criteria described here may help develop operational guidelines for recognizing, and thus helping aircraft avoid dangerous storms.

The effects of various FAA radar parameters and selectable operating modes were described in the Phase I NSSL report by Zittel, with emphasis on airport surveillance radars (ASR). These considerations also are generally applicable to the air route surveillance radars (ARSR), while recognizing

Table 1. Comparative Radar Beam Characteristics

Type	Normal Antenna Tilt	Beam Shape (Width, Gain) θ , Horizontal ϕ , Vertical	Expected one-way signal loss at specified altitudes, at 150 km range, with antenna at normal tilt angle. HT = 1 km HT = 5 km HT = 10 km
WSR-57	Variable, but normally 0.5°	Conical 2°, 38.5 dB	.3 dB 2.7 dB
ASR-5	Fixed, normally at 2.5°	CSC ² , $\theta = 1.5^\circ$, $\phi \sim 5^\circ$ 34 dB	3.1 dB .3 dB 1.0 dB
ASR-8 (low)	Fixed, normally at 2.5°	CSC ² $\theta = 1.35^\circ$, $\phi \sim 5^\circ$ 33.5 dB	3.4 dB .3 dB 1.0 dB
ARSR-1L*	Fixed, normally at 3°	CSC ² $\theta = 1.35^\circ$, $\phi \sim 6^\circ$ 34.3 dB	2.3 dB .4 dB .6 dB
ARSR-2	Fixed, normally at 3°**	CSC ² $\theta = 1.2^\circ$, $\phi \sim 4^\circ$ 34 dB	5.1 dB .7 dB .5 dB

* The ARSR-1L designation utilized in this report is actually known in FAA as ARSR-1D.

** For antenna pattern lower -3 dB point on horizon, tilt would be 2°.

their lower PRF (nominally 360) and lower antenna rotation rate (5-6 RPM). This report examines the FAA radars with their present characteristic parameters and selectable operating modes. The inherent capabilities of various FAA radars for weather detection in comparison with the WSR-57 performance has been studied through simulation and analysis of some field measurements by the Applied Physics Laboratory (APL), of the Johns Hopkins University, and the report is expected to be published soon. In the APL study, the FAA radars utilized operational modes and adjustments optimized for weather performance. An overall way being considered by the FAA for improving the weather performance of their existing and planned new model ATC radars, for replacement and establishment of newly qualified facilities, is the incorporation of a separate weather receiving channel that would be designed for best possible detection and calibration of especially the more intense reflectivity levels. The weather returns would bypass the significant weather reduction effect of the circular polarization mode, when it is operationally selected to enhance aircraft detection during precipitation. The weather degrading effects of the STC waveform that is adjusted differently at each radar site for best aircraft target detection would be eliminated. Special ground clutter filtering would be designed for ground and slowly moving clutter suppression coupled with best possible performance of calibrated weather received over ground clutter. It may even be possible with some models of airport surveillance radars to minimize multiple trip weather if the PRF of one of the two dplexed radar channels, utilized for weather, was automatically lowered during troublesome periods; or the multiple trip weather could perhaps be automatically sensed and eliminated. When and if certain weather performance improvement modifications are incorporated, operational guidelines may need to be reconsidered. This report may also be helpful in pointing out the desirability for incorporating selective modifications.

Almost all FAA air route surveillance radars utilize the narrower-beam characteristics of the ARSR-2. The figures in this report are for the wider-beam ARSR-1L (1D) antenna characteristics. Comparisons of the weather performance of the ARSR-1D and ARSR-2 radars are included in the above referenced APL report; and the weather performance differences should be considered in the development of the operational guidelines.

2. PAST RESEARCH AND RELEVANT FINDINGS

First, it should be emphasized that accurate measurement of precipitation rate and detection of hail are extremely difficult even with a carefully calibrated narrow beam meteorological radar, because the precipitation particle parameters which determine radar reflectivity are not uniquely related to precipitation mass. With FAA radars optimized for detection of aircraft by use of wide vertical beams, precipitation measurement is more difficult because the return indicated at any point on the plan-position display actually represents an average over a large vertical depth. Controllers must always be aware of the coarseness of their radar's beam in searchlighting storms--and realize that as storm range increases, the radar is sampling a larger volume with gradual loss of the detail that may be needed to identify severity.

By using guidelines for severe storm recognition, and by making judicious use of other weather observations, thunderstorms hazardous to aircraft should usually be identifiable without exact reflectivity measurements. However, to provide an increased margin for safety, criteria for severe storms are lowered to include all storms of moderate intensity and higher; this procedure slightly reduces the airspace deemed suitable for flight by en route aircraft.

Recent tests of radar displays remoted from Air Traffic Control (ATC) radars to Flight Service Stations in Texas and Oklahoma have shown that enough information can be provided over voice grade telephone links to guide general aviation aircraft (without onboard radars) around storms [Wilk, 1976]. Of course, severe storms in the Southwest usually have very high tops, are well organized and contain a volume of rain and hail sufficiently large to fill (or nearly fill) even the broad beams of ATC radars. Thus, reflectivity displays of these large storms during their mature stage are similar to their display on the NWS WSR-57 radar, to a range of at least 60 n.mi. (111 km).

Other types of storms and rainshowers are perceived differently by the fan-beam ATC radars and the cone-beam WSR-57 and 74 radars. When the atmosphere is abnormally unstable (usually because of rather cold air aloft) and there is insufficient moisture to create large areas of heavy rain, storms with very strong updrafts may still produce hail, dangerous turbulence and tornadoes, with modest reflectivities at ground level. In this case, the ATC radars may perceive strong reflectivities aloft while the WSR radars scanning in azimuth at low elevation angles, perceive lesser reflectivities. On the other hand, when tropical cyclones or low-level jet streams carry copious amounts of water vapor inland, large convective rainshowers may produce strong echoes both on WSR and ATC radars. Although no hail or strong wind gusts occur, rain and turbulence may adversely affect passenger comfort; though rarely do such showers require the National Weather Service to issue public warnings.

By knowing air mass characteristics which accompany (cause) the rain and associated radar echoes, a controller can better interpret the meaning of reflectivities being displayed, and probably will anticipate severe weather. This interpretation is explored further in section 3.

With this brief outline of characteristics of storm and echo growth, there are several previous studies which provide insight concerning strengths and shortcomings of ATC radars for accurate and timely display of storm reflectivities.

In 1971, Pell analyzed 10-dB intensity contours of radar images from hailstorms in Alberta, Canada (measured with an AN/FPS/502 radar at RCAF station Penhold). Like FAA ATC radars, this 10-cm radar has a narrow horizontal beam (1.2 deg.) and a wide vertical beam--in fact, three wide vertical beams of 5, 7, and 9 deg. with each beam axis tilted to provide a small overlap. For comparison, he also had data from a very narrow conical beam radar (0.75 deg.) which was tilted sequentially at 0.5 deg. intervals. The storms

Pell studied produced golf-ball sized hail and peak reflectivities of 50 dBZ. By comparing and summing the contoured reflectivity data (constructed manually from film sequences) for the three broad beams and the narrow beam radars, he determined that the composite view of total storm reflectivity was a very useful measure of storm severity. One such storm is illustrated in Figure 1.

A short time later, Pell's conclusion gained support when Greene and Clark [1971] compared vertically integrated reflectivity data with severe storm occurrences in Oklahoma. All concluded the total contribution of high liquid water content plus hail suspended aloft causes the vertically integrated reflectivity to be a precursor of severe weather events at the surface.

In 1978, Dobson et al. examined the effect of vertical integration theoretically by superimposing severe storm reflectivity profiles (obtained with relatively narrow, conical beam radars) on the broad beam patterns of FAA ATC radars. This study shows that detection by the ATC radar of strong reflectivities aloft in severe storms leads to larger reflectivities than perceived via narrow beam radars which illuminate low altitudes especially at short range.

Finally, operational tests at Midland, Texas, and Oklahoma City Flight Service Stations, have confirmed that ARTCC (or ARSR) radars can provide sufficient information to locate most dangerous storms [Wilk, 1976].

Now the question arises--can approach control radars, with slightly wider beam patterns and hence slightly less accurate reflectivity estimates than ARTCC radars, also provide adequate warning? To answer this question, we must establish reflectivity thresholds for the storms; which will in turn establish critical vertically integrated reflectivity values for the ASR radar. Of course, these values degrade in the presence of other weather suppression characteristics of the radar's mode of operation, i.e., circular polarization (CP) and Moving Target Indication (MTI).

Once we establish the expected reflectivity profile(s) of severe storms, and the average rate of development from first echo, we can predict whether, when, and at what range the ASR (and ARSR) radar echoes signal the controller of hail and possibly other hazards.

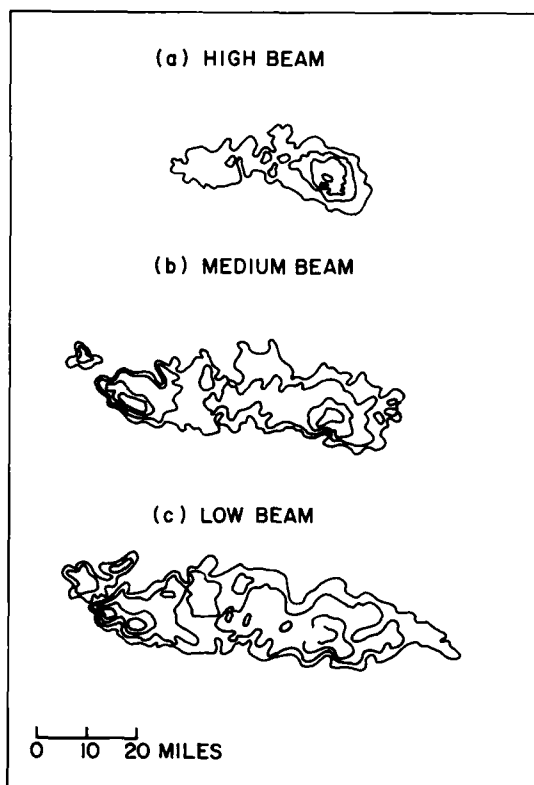


Figure 1. Vertical distribution of precipitation as seen by a multiple-beam, air traffic control radar [after Pell, 1971].

NSSL's data from individual severe thunderstorms are very helpful in defining reflectivity profiles since they are judged typical of the very large storms which produce tornadoes; but research findings concerning lesser storms and structures typical of other geographical areas are equally important, especially where radar echo intensities have been related to contemporaneous characteristics of the air mass. For example, Hamilton [1966], using the 3-cm radar at McGill University, relates the height of precipitation accumulation (Z_e maximum) in northern latitude thunderstorms to updraft velocity and energy of convection (thermal buoyancy) derived from atmospheric soundings.

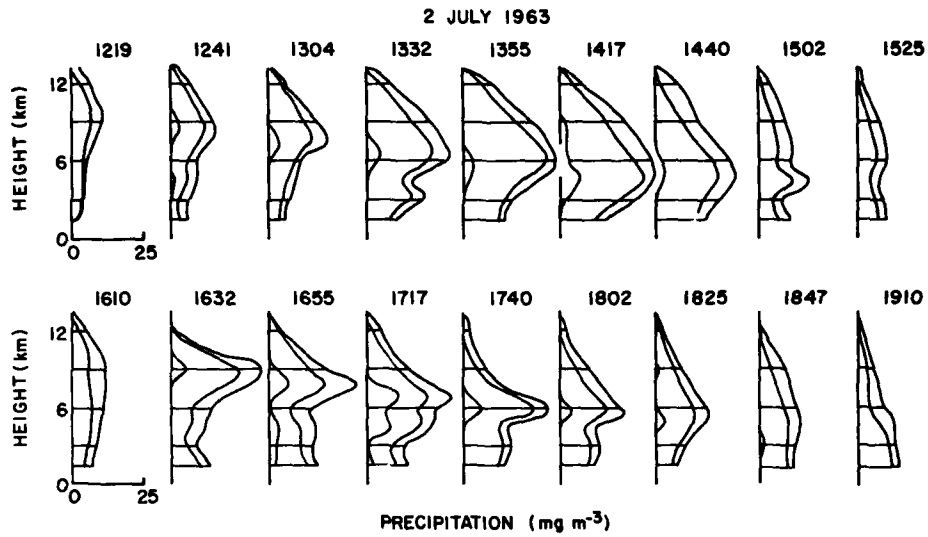
Hamilton's precipitation profiles (figure 2a) show also the development and gradual descent of heavy rain which accumulates during early stages of storms when updrafts are very strong. Analysis of the areal coverage of radar reflectivity as a function of height, and in relation to surface hail occurrences, supports the conclusion that radar echoes (first precipitation) in most severe storms begin several thousand feet above the altitude where particles can freeze, and then intensify quickly. In fact reflectivities may exceed 30 dBZ before the rain (echo) has descended below cloud base. Aircraft penetration of Colorado storms confirms hail within clouds during early stages of storm development.

Paraphrasing the description of Dennis et al. [1970], of radar observations of severe hailstorms in South Dakota (figure 2b)--"echoes appear first in new cloud growth at 32,000 ft (10 km). Radar intensity exceeds 50 dBZ before the peak begins to descend, suggesting considerable concentration of precipitation temporarily supported by strong updrafts. The rates of descent vary, but typically are about 10 m s^{-1} (1900 ft min^{-1}). Thus, the peaks arrive at the ground in 15-25 min."

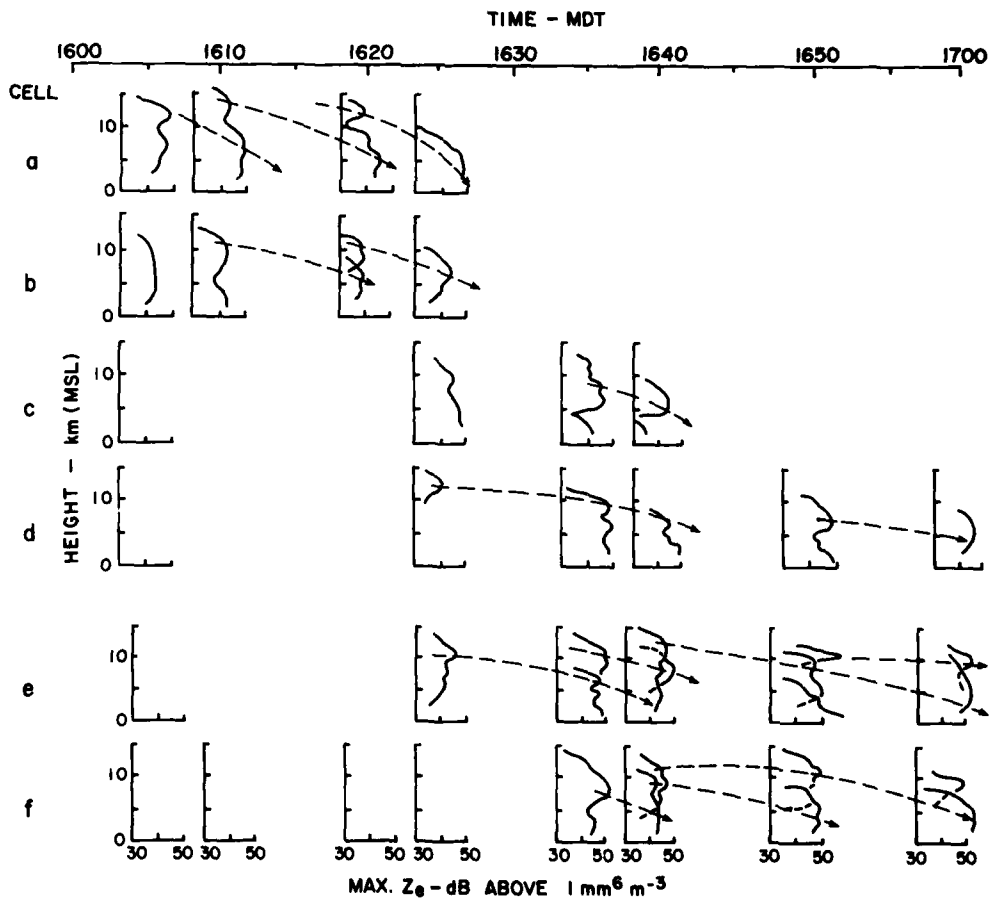
As noted by Smith et al. [1975], most numerical models of clouds indicate higher reflectivity gradients than those actually observed--partly because the limited spatial resolution of radar systems smooths the actual gradients.

2.1 First Echo Characteristics

Generally, first precipitation in convective clouds forms in updrafts where the temperature is 0° to -10°C . The liquid cloud droplets, though at a temperature below the freezing point, are accreted rapidly by the first raindrops and frozen particles, which increase within a few minutes to yield the first echo. This echo, following the vertical and horizontal expansion of the newly formed precipitation, grows quickly as more and more of the radar beam is filled with an increasing number of large raindrops. The rate at which the first echo grows in size and intensity depends essentially on the strength of the updraft and the cloud density [Kessler, 1974]. Also, it has been observed that the higher the first echo forms, the more likely it is that severe weather (hail, tornadoes, and strong outflow) will follow. Donaldson [1961] indicated this first with radar reflectivity profiles of storms in New England.



(a)



(b)

Figure 2. Examples of vertical profiles of precipitation return and their descent with time [after Hamilton, 1966, and Dennis et al., 1970].

Several studies have shown the statistical distribution of first echoes from developing nonsevere thunderstorms. Johnson and Dungey [1978] found, in studying convective clouds in Missouri, the majority of first echoes appear between 7500 ft (2 km) and 15,000 ft (5 km). Figure 3 summarizes their findings in projects Whitetop and Metromex. In 1976, Carbone et al. published similar results from observing first echoes in Texas (figure 4). Both studies show strong tendencies for precipitation within nonsevere convective thunderstorms to develop first at, or slightly above, the freezing level, and to grow upward and downward at about 500 ft/min. (2.5 m s^{-1}), and 1500 ft/min. (7.6 m s^{-1}), respectively. Johnson and Dungey [1978] summarize this initial growth schematically as a parabolic time-height evolution (figure 5). The apex (beginning) of this growth profile is between the 0°C level and an upper bound of about -40°C , above which unfrozen cloud rarely exists.

Carbone et al. [1976], in the same report on first echo growth, described the initial development of two contrasting thunderstorms, where first echoes appeared at 17,000 ft (5.3 km) and 27,000 ft (8.3 km) with corresponding temperatures of -6°C and -27°C and later development of maximum reflectivities of 52 dBZ and 67 dBZ, respectively. The characteristics of these echoes are similar to those observed on NSSL radars in central Oklahoma, i.e., intense, but nonsevere storms develop first echoes between 0° and -10°C , with maximum reflectivities briefly greater than 50 dBZ, while severe storms develop first at a much higher altitude and produce a large area of echo greater than 50 dBZ, and maximum reflectivities often exceed 60 dBZ.

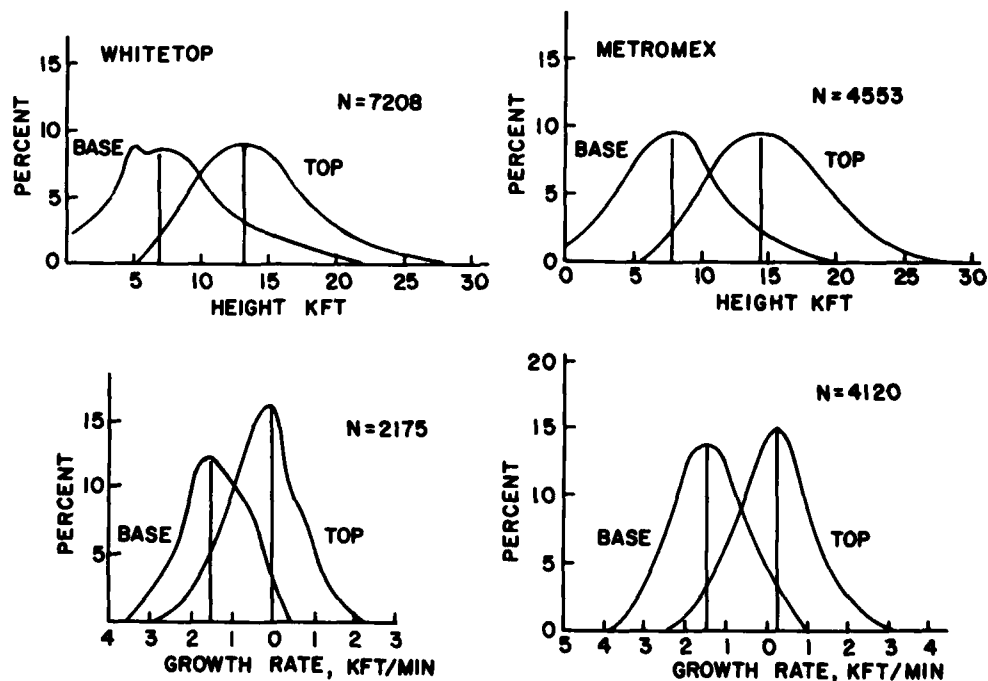


Figure 3. Frequency distributions of first echo bases, tops and vertical growth rates observed in nonsevere storms in projects Whitetop and Metromex (Missouri) [after Johnson and Dungey, 1978].

Study of upper air parameters at the time of tornadoes [David, 1976] shows that the freezing level and most first echoes on severe storm days occur between 13,000 ft and 14,000 ft (about 4.3 km). But the few which develop into severe storms begin much higher--20,000 ft--30,000 ft (6-9 km). Development time for the marginally severe thunderstorms may be as short as 15 minutes--but storms capable of producing large hail and tornadoes probably take 40 to 50 minutes to fully develop vertically and to produce the heaviest rain at the ground. The first echo (from severe storms) typically develops maximum intensity of 30 dBZ within five minutes, exceeds 50 dBZ intensity within 15-20 minutes; and another 15-25 minutes elapses during vertically spreading with descent to the ground.

Probably the highest initial echoes observed in thunderstorms which subsequently became severe, occurred in the Black Hills, South Dakota storm of July 17, 1968 [Dennis et al., 1970], in the Union City, Oklahoma storm of May 24, 1973 [Brown et al., 1976], and the Colorado storm of June 22, 1976 [Harris and Fankhauser, 1978]. All of these extremely well-documented storms developed precipitation initially much above the environmental freezing level.

In summary, the development "window" that forecasters and controllers should monitor for storm origin is a vertical airspace about 16,000 ft (4-6 km) deep, beginning 15,000 ft (4-5 km) above terrain. In terms of radar sampling volume, this corresponds to a beam axis tilt from about 6.5 deg. at 20 n.mi. (37 km) to 0.5 deg. at 110 n.mi. (204 km). Beyond 110 n.mi. (204 km), the beam of the Weather Service's WSR-57 radar is no longer filled and significant degradation of signal begins to occur. The same effect with the Air Traffic Control radars begins at approximately 55 n.mi. (102 km), partly because of wider beams, and partly because of the mechanical tilt of the antenna. Of course, the maximum operational range of ASR radars is about 60 n.mi.

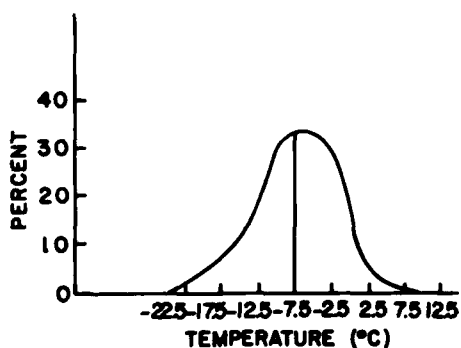


Figure 4. Approximate temperatures at heights where first echoes form in nonsevere storms in Texas [after Carbone et al., 1976].

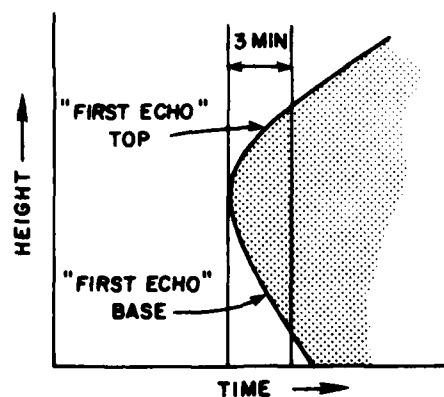


Figure 5. Schematic illustration of the time-height evolution of the radar echo from nonsevere storms [after Johnson and Dungey, 1978].

2.2 Relation of Storm Pattern on NWS Radar Reports

Like most weather observations, radar reports are "snapshot" summaries of the state of the atmosphere as it exists at observation time. For example, surface wind direction and speed may be representative of only the last few minutes, and variations in speed are noted by reporting gustiness. The hourly radar reports are often structured to present salient characteristics of the overall field of echoes. Thus, echo strength, movement, and height may be selected for reporting because they represent extreme values indicative of severe weather, or because they are judged to be representative of the entire precipitation field. It is not possible for observations taken manually once or twice an hour to depict all individual thunderstorms and their growth patterns accurately. In fact, when the radar operator observes strong echoes on the PPI and stops the antenna rotation momentarily to scan the storms vertically, the observed reflectivity profiles may differ considerably, depending on the age of each storm surveyed.

This variation of storm height and intensity is summarized statistically (figure 6) in data obtained from five WSR-57 radar sites of the National Weather Service in August and September, 1965. These data were taken on special request by NSSL to compare maximum reflectivity and storm top height—to determine the expected error in estimating height from surface reflectivity. The standard deviation of echo height estimated from intensity varies from 5 to 8 thousand feet (1.5 to 2.5 km).

The rates at which echoes grow and descend vary with air mass structure, which, in turn, varies seasonally and geographically. The later is illustrated in the analysis of the standard deviation of echo tops vs reflectivity for 29 WSR-57 radars—a one-month sample (figure 7). The coastal data show much greater scatter than those of the high plains. The northward extension of high values near St. Louis (STL) probably reflects the seasonal penetration of low-level Gulf moisture associated with the storm tracks for the few storm days during that particular 30-day period.

3. EFFECT OF BEAM PATTERNS ON STORM DETECTION

Six thunderstorm models were selected to estimate relative performance of FAA and Weather Service radars in storm detection, using observed vertical profiles of reflectivity and statistical findings of height of first echo growth (cited in section 2). The growth and descent rates of the precipitation (figure 8) are commensurate with the statistical data and the single case studies quoted earlier. Color photographs of PPI displays of several storms observed with the narrow beam (0.8 deg.) NSSL Doppler radar are included to illustrate differences in reflectivity structure and rate of development. These data were collected during the Joint Doppler Operational Project [JDOP Staff, 1978].

Echo growth rates vary with the strengths of updrafts and downdrafts. The cases shown here illustrate typical time spans of vertical growth. Six time steps of ten minutes were used to produce the vertical reflectivity

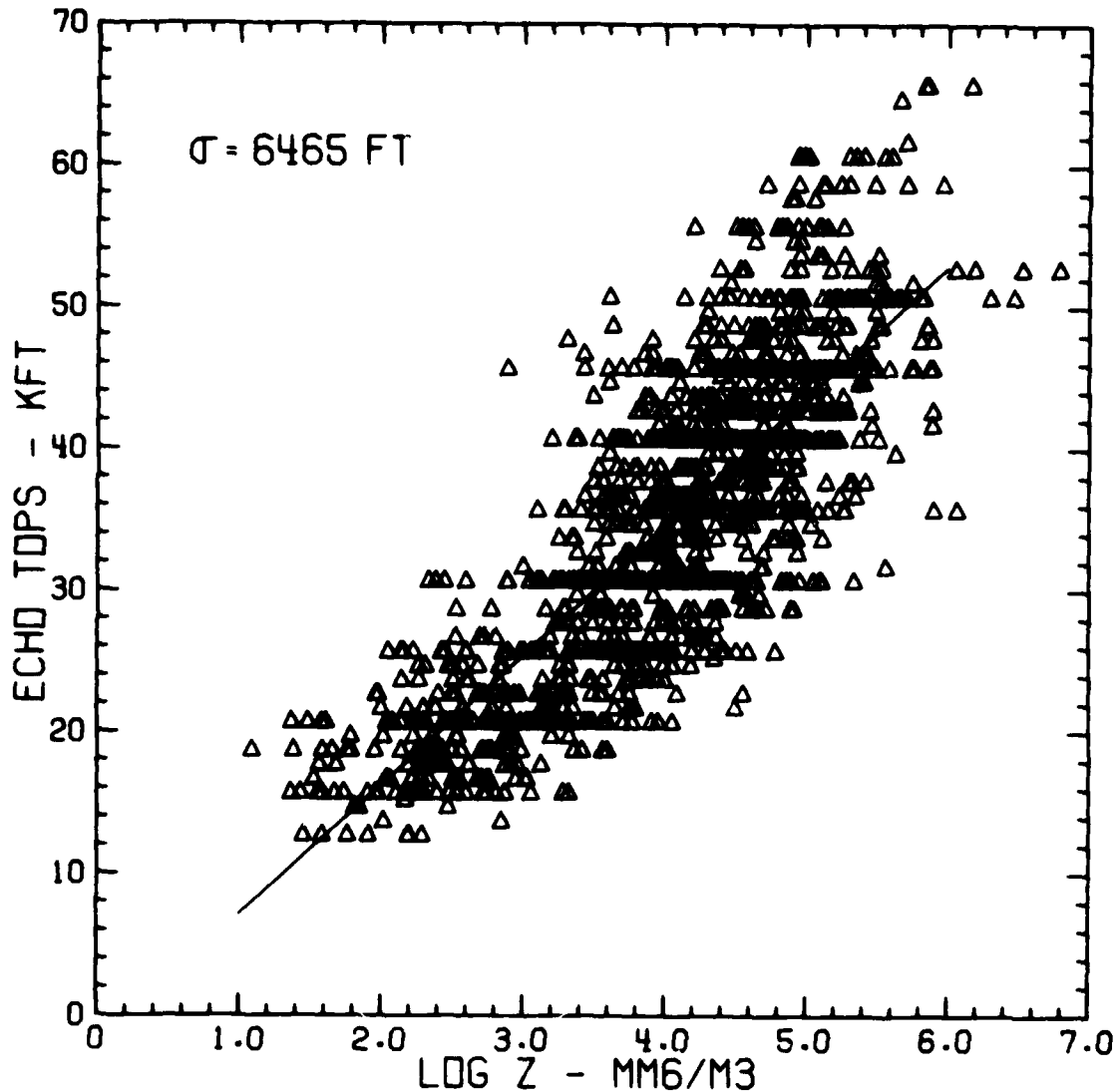


Figure 6. Composite of "snapshot" measurements of maximum echo height and surface reflectivity for 1305 observations made at five WSR-57 radar sites.

profiles shown in Figure 9. Appendix B includes data on the model reflectivity vs height profiles at the time steps. Models 1 and 2 are combined to represent those showers and thunderstorms that occur most often but never produce severe weather. For simplicity, Model 2 is ignored in the discussion, and its characteristics are assumed to be implicit between the discussions of Models 1 and 3. Model 3 represents a type of storm seen in Oklahoma in early spring, when wintertime cold temperatures aloft and strong winds are still occurring, and the air mass is destabilized by sudden influx of warm air from the Gulf. The damage producing storm of April 5, 1978, observed near Hennessey, Oklahoma is shown as an example (figure 10).

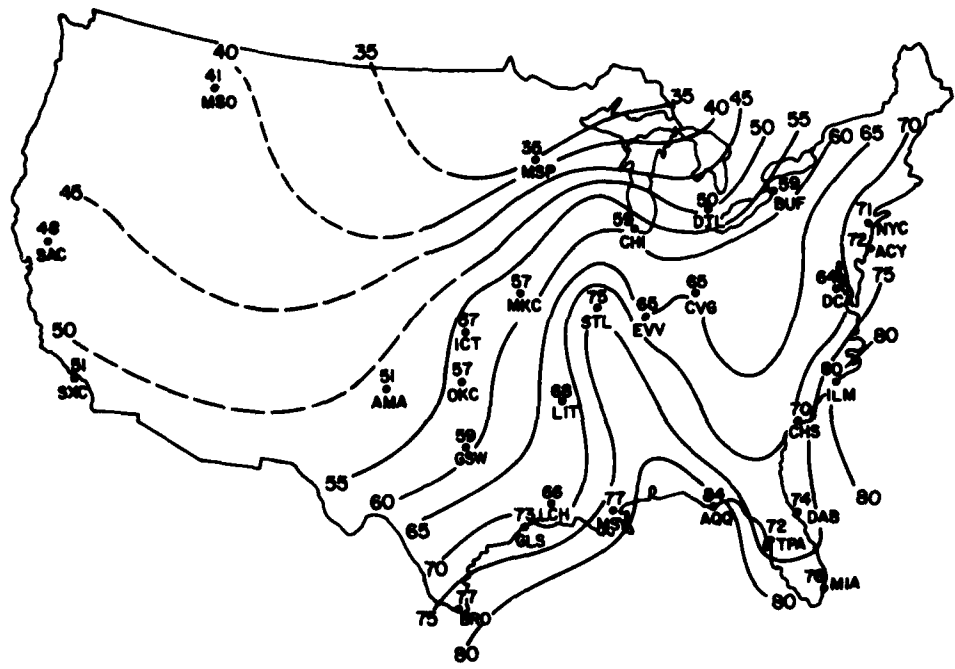


Figure 7. Geographical changes in the variation of echo height surface reflectivity measured with 29 NWS, WSR-57 radars for a selected one-month period in August 1965.

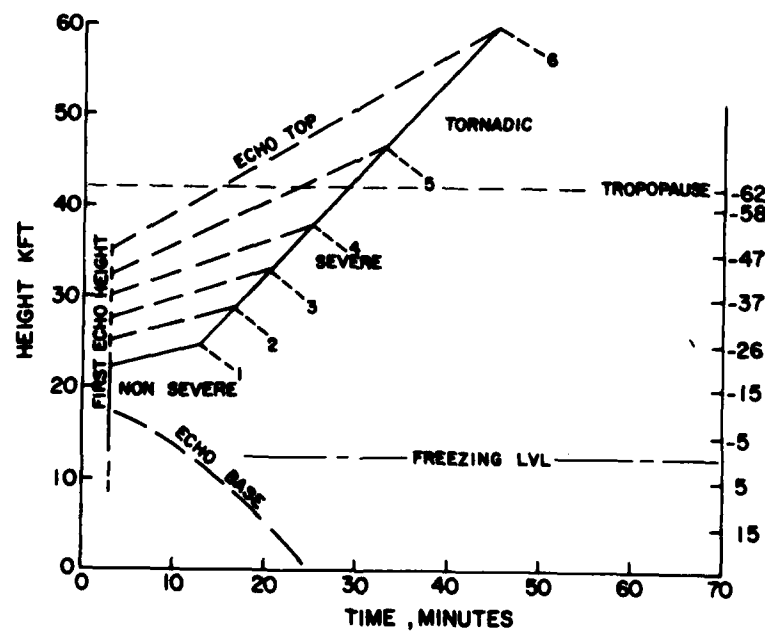


Figure 8. Precipitation growth and descent patterns used to simulate reflectivity profiles for determining effects of beam patterns of NWS and FAA radars.

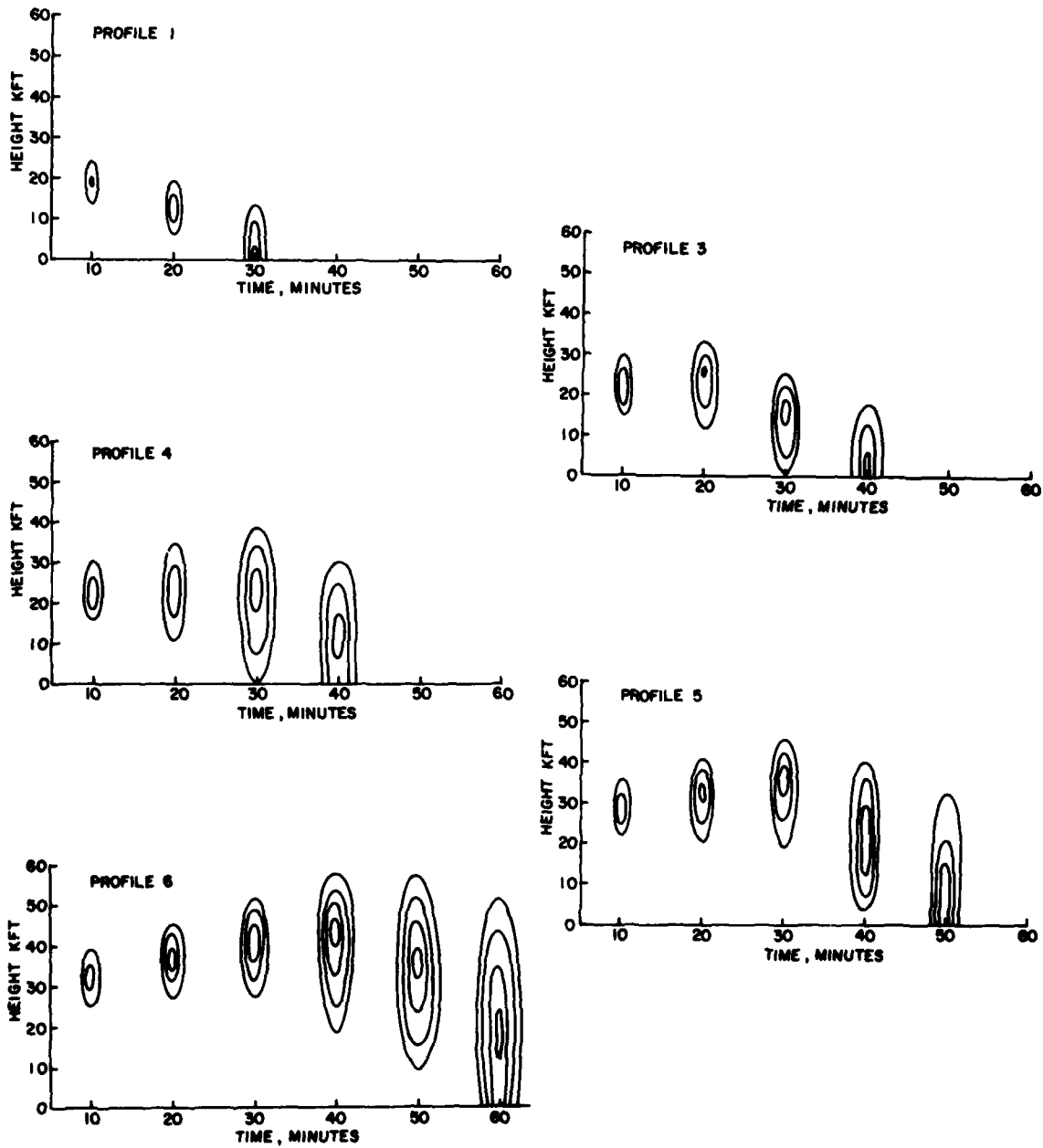


Figure 9. Vertical reflectivity cross sections used to represent initial echo growth in storms of increasing severity.

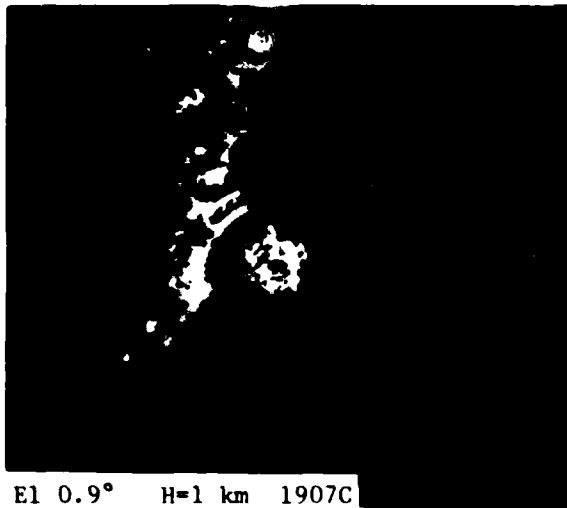
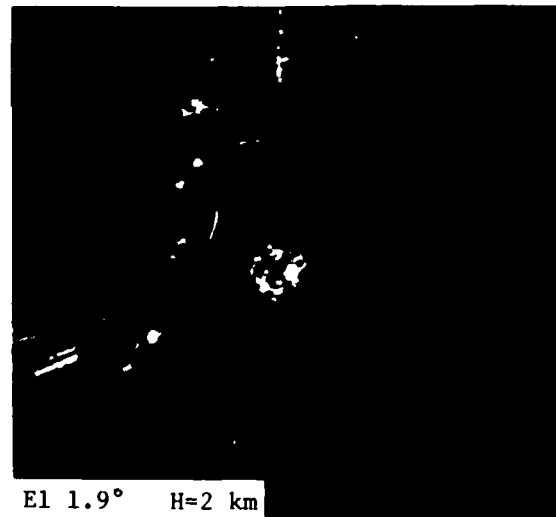
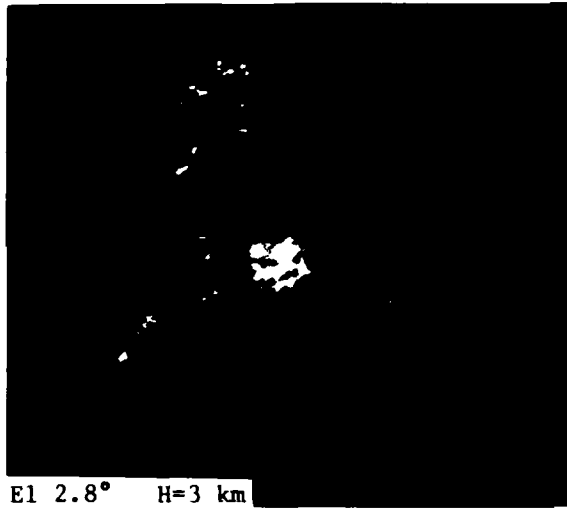
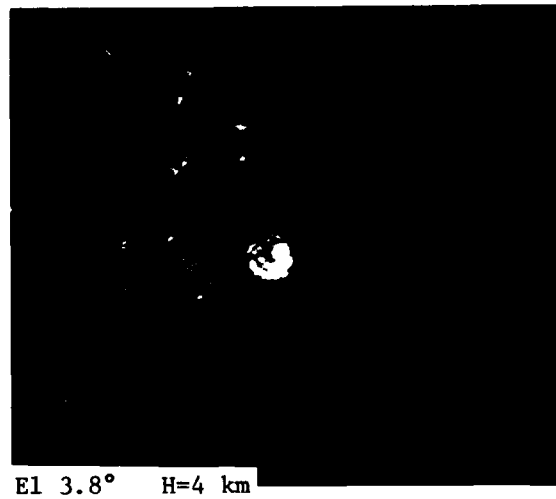
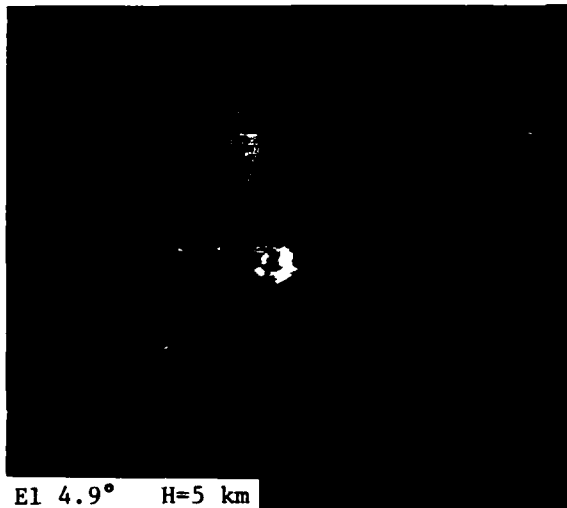


Figure 10. Reflectivity data from the narrow beam (0.8 deg.) NSSL Doppler radar, showing the relatively low tops and low maximum reflectivities associated with marginally severe thunderstorm (Model 3). See caption of Figure 11a for color reflectivity levels. "H" is height of estimated storm centroid.

At the other end of the spectrum, the storm designated as Model 6 represents those extreme, and fortunately rare storms which produce mammoth hail and large tornadoes. The Union City, Oklahoma storm of May 24, 1973 is probably the best documented of this class of storm, although many other studies of similar cases exist. Severe hailstorms, which fall in categories of storm models 3, 4, and 5, are described abundantly in the literature [Marwitz, 1972]. A recent example, which occurred in Oklahoma on April 29, 1978, is shown in Figures 11a, b, and c.

The procedure followed in simulating radar detection and measurement of these six storms closely resembles the technique used in a recent study of FAA radars by Dobson et al [1978], which compares performances of the NWS WSR-57 radar with ASR and ARSR ATC radars. They found the wide beam FAA radars actually surpass the narrow beam WSR-57 radar (operating at 0.5 deg. tilt) out to a range of 85 km, when the storm reflectivity peaks above 10,000 ft (3 km). At ranges beyond 45 n.mi. (85 km), the performance begins to degrade below that of the WSR-57 radars.

The principal refinement in this study is to include a time sequence in the development of the echo, to compare first radar detection of large reflectivities in both time and range. The calculated responses of ARSR, ASR and WSR radars to selected storm profiles at specified times and ranges are included in Appendix A. In the analysis of mature storms we expect to see effects similar to those found in our earlier studies [Wilk et al., 1965; Zittel, 1976] where the performances of the ARSR, ARTCC radars were deemed sufficiently accurate for severe storm surveillance. But how well do FAA radars see developing storms, and what is the effect of range and altitude on detection of first development? Early detection is very important because National Weather Service warnings are not always fully disseminated to FAA facilities before storms have matured and a danger (to flight) may exist for tens of minutes during early lifetimes of severe storms.

Model 1 - Nonsevere Thunderstorms

The most recent, and probably the most thorough study of radar echoes from nonsevere showers and thunderstorms is the study by Konrad [1978]. With data from the very high resolution SPANDAR radar at the Wallops Island Facility, he determined frequency distributions of storm intensities with altitude, and the mean profiles of reflectivity for various categories of surface reflectivity (figure 12). Additionally, Konrad concluded that reflectivity maxima rarely occur above 13,000 ft (4 km) in nonsevere storms, and the mean reflectivity is less than 45 dBZ above an altitude of 20,000 ft (6 km). This is significant because it confirms, with a very large sample, conclusions initially drawn from case studies that reflectivity maxima aloft are indications of hail (figure 13). This is substantiated also by recent findings in South Africa [Mather et al., 1976] that hail is not likely unless the 45 dBZ contour extends above 25,000 ft (7.5 km), where the warm season temperature is about -20°C (figures 14a and b).

The reflectivity profile in our model 1 storm (figure 9) is fashioned to represent the median of the nonsevere, convective thunderstorm, which develops randomly in the conditionally unstable air mass. Sometimes the

individual cells amalgamate to form a multicell cluster, which persists for an hour or more. Even then, the radar echo profile shows heavy rain only below 13,000 ft - 16,000 ft (4-5 km), and no severe weather occurs.

Radar detection and measurement of this type of storm is summarized in Figure 15. In our analysis, the antenna gain (G) and the model reflectivity (dBZ) are used to determine the relative meteorological power factor (MPF), defined as

$$MPF = \frac{\sum_{i=1}^N G_T(\phi_i) G_R(\phi_i) \Delta\phi Z_{dBZ}}{\sum_{i=1}^N G^2(\phi_i) \Delta\phi}$$

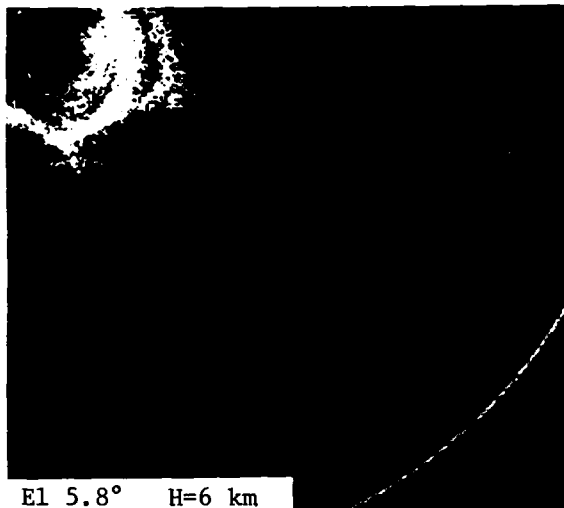
The WSR-57 radar measures the true meteorological power of the storm at maturity (time step 3) to a range of 20 n.mi. (37 km). Beyond that range, the radar underestimates storm intensity by about 10 dB at 65 n.mi. (120 km) and by 30 dB at 110 n.mi. (204 km). Beyond 130 n.mi. (240 km) the radar does not detect this storm. In contrast, the FAA ARSR-1 shows discrepancies of 13 dB and 34 dB. The ASR-8 low beam underestimates by up to 10 dB over its 60 n.mi. operational range as compared to the WSR-57.

Considering the growth profile of this nonsevere storm model, and the response of the radar gain profiles, the following general conclusions are drawn from numerical analyses of this model:

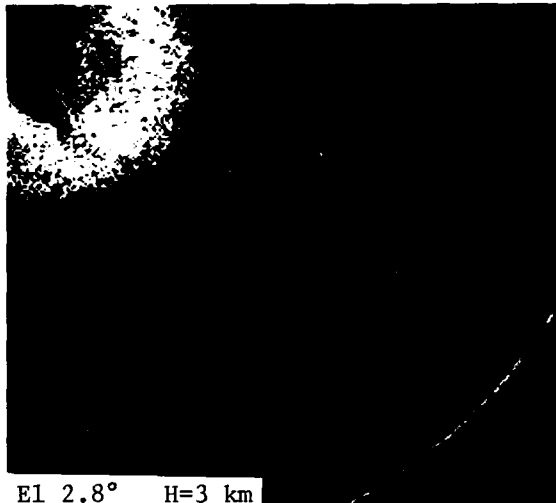
1. The intensities of nonsevere showers and thunderstorms are underestimated by approximately 3 dB by the ARSR and by up to 10 dB by the ASR as compared to the WSR.
2. The range dependence of echo intensity from 10 n.mi. to 60 n.mi. (~20-110 km) on the ASR radars is about $R^{-2.1}$.
3. All showers and thunderstorms of this type are undetectable by both ARSR and NWS radars beyond about 130 n.mi. (240 km).
4. For the assumed rate of growth, the nonsevere storm is seen best by NWS and FAA radar during the period of maximum development (time step 2).

Models 3 and 4 - Strong to Severe Thunderstorms

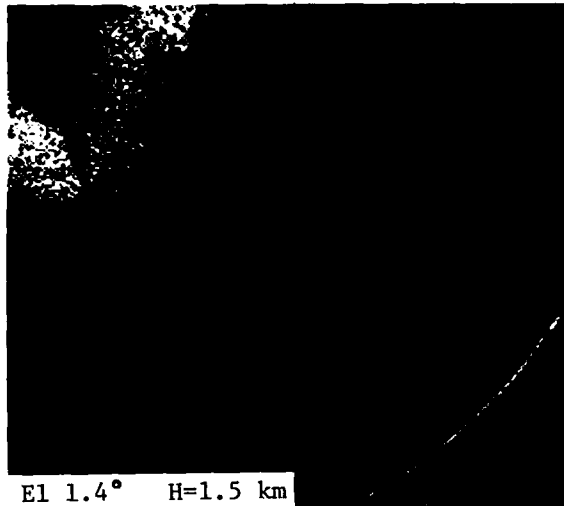
These classes of storms represent the most common severe thunderstorms, which produce the large number of reports of light to moderate damage to property and crops. They are usually easy to circumnavigate, but are dangerous to aircraft that penetrate within the cloud boundary or that attempt landings or takeoffs within a few kilometers of the storm. The storm's radar echo (precipitation) usually develops first between 20,000 and 25,000 ft (6.0-7.6 km) and reaches the ground about 30 minutes after first detection.



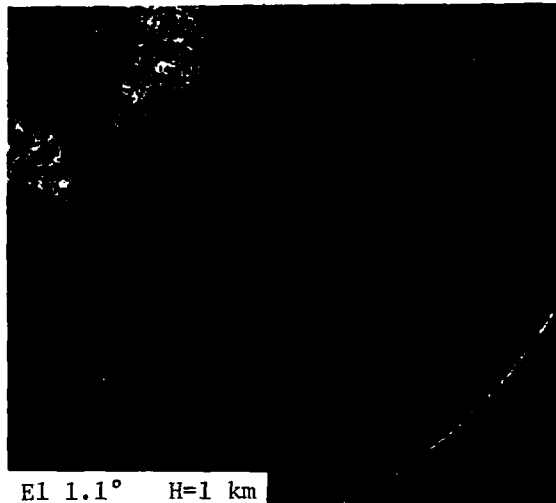
El 5.8° H=6 km



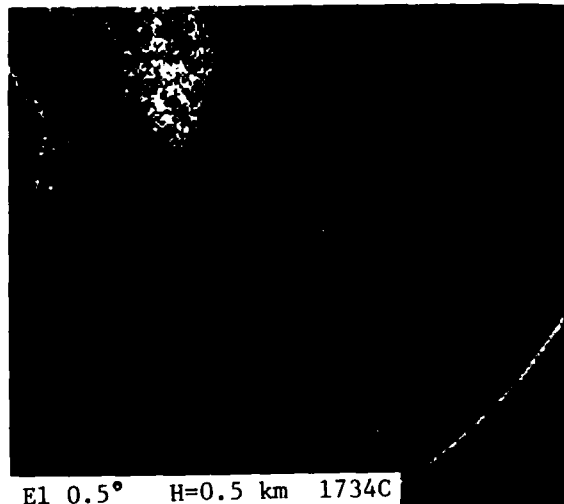
El 2.8° H=3 km



El 1.4° H=1.5 km

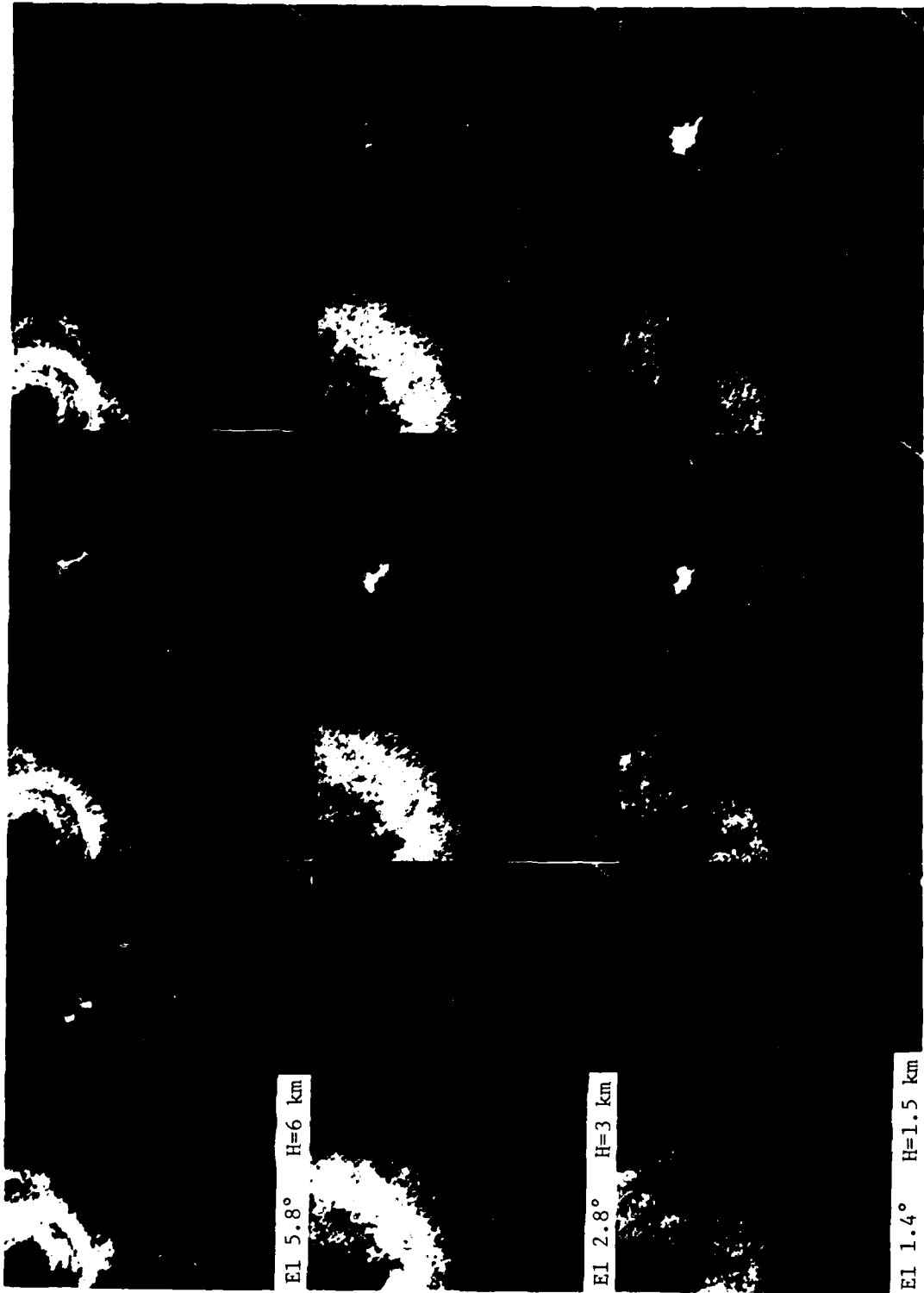


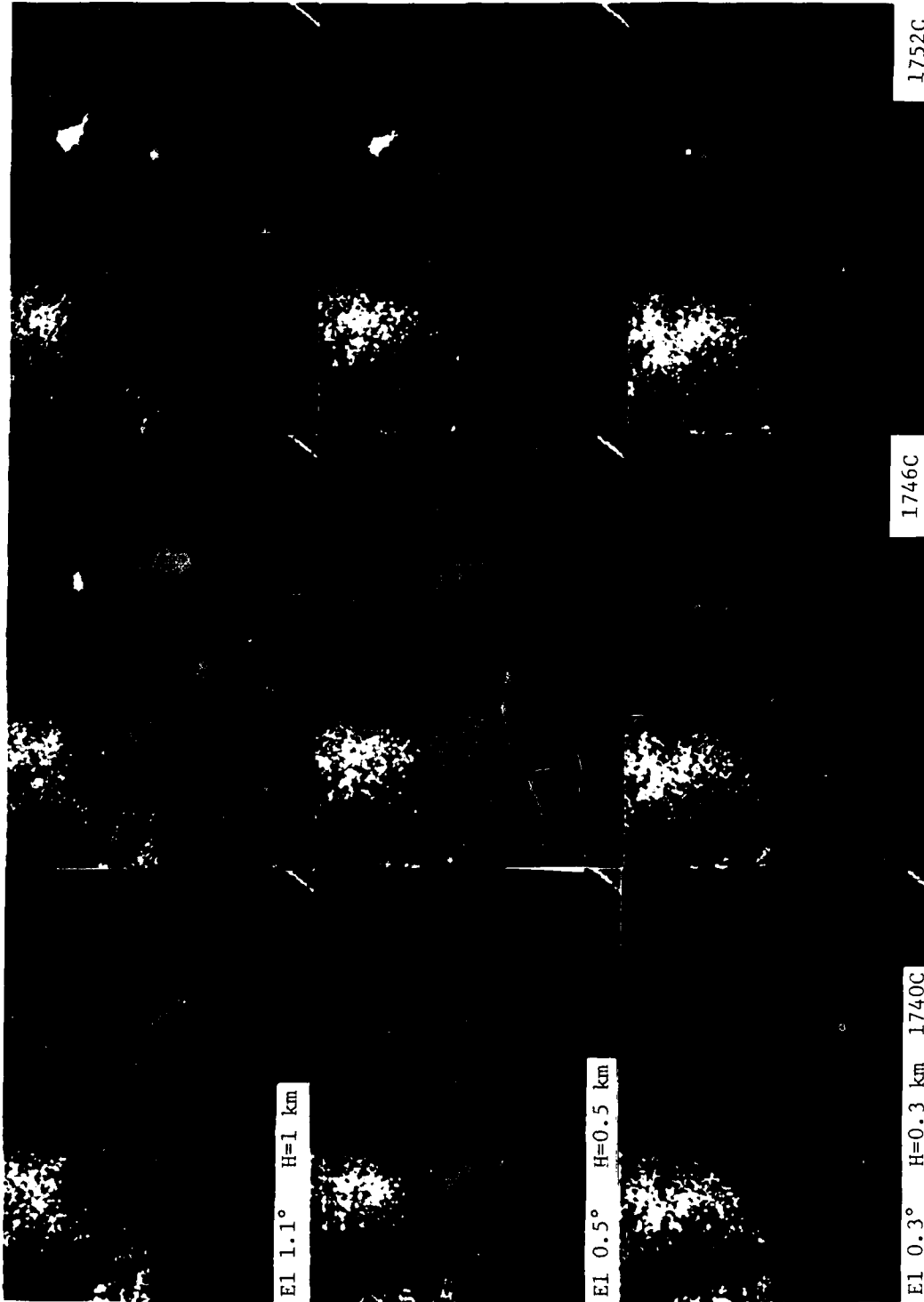
El 1.1° H=1 km



El 0.5° H=0.5 km 1734C

Figure 11a. Development of first echo on NSSL's Doppler radar, from the storm which later (fig. 11c) produced large hail at Ada, Oklahoma, 29 April 1978. Contours in all photographs conveyed reflectivity levels of below 25 dBZ (grey), 25-30 dBZ (cyan blue), 31-33 dBZ (blue), 34-40 dBZ (blue-violet), 41-45 dBZ (black), 46-50 dBZ (pink), 51-55 dBZ (yellow), 56-60 dBZ (green), 61-65 dBZ (red), above 65 dBZ (white).



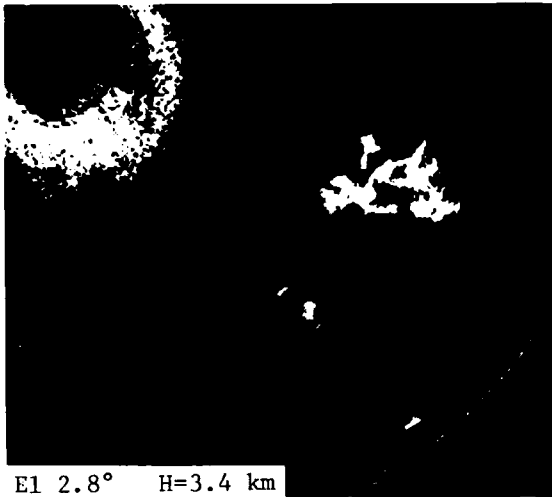


1752C

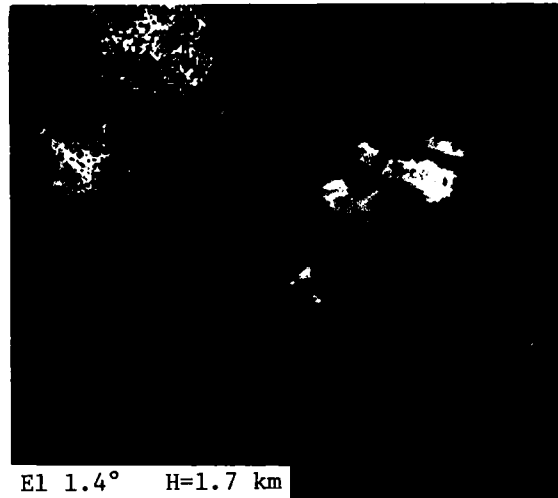
1746C

1740C

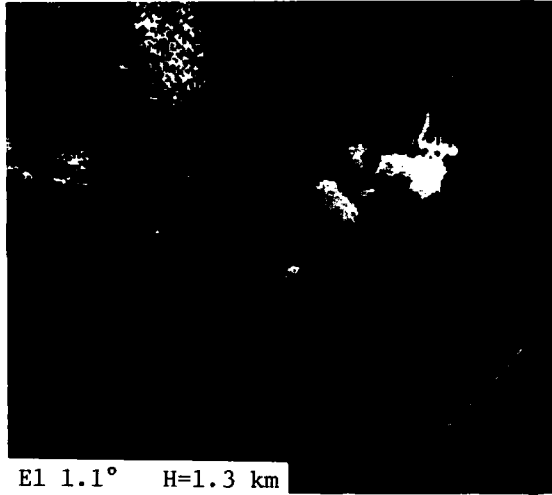
Figure 11. Three vertical intensity profiles at 6 minute intervals, showing descent of area of equal greater than 45 dBZ (pink) during early development of a severe hail storm near Abil, Oklahoma, 23 April 1978.



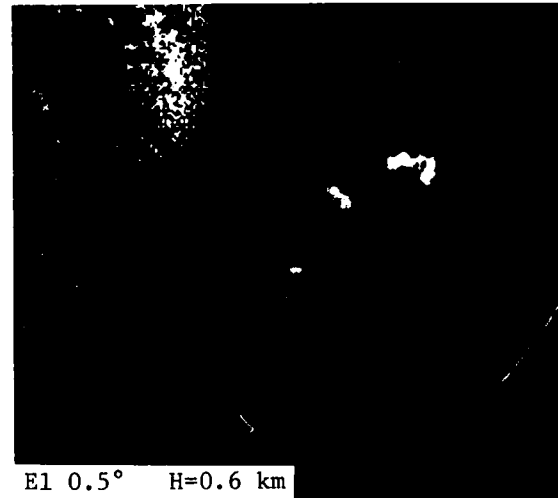
El 2.8° H=3.4 km



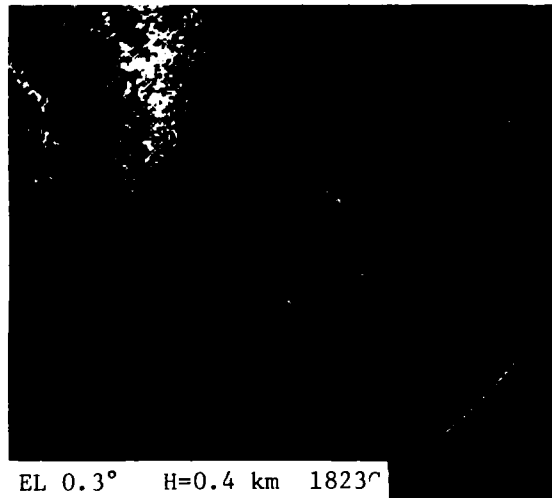
El 1.4° H=1.7 km



El 1.1° H=1.3 km



El 0.5° H=0.6 km



EL 0.3° H=0.4 km 1823⁰

Figure 11c. Mature stage of echo development from the Ada, Oklahoma hailstorm, 29 April 1978.

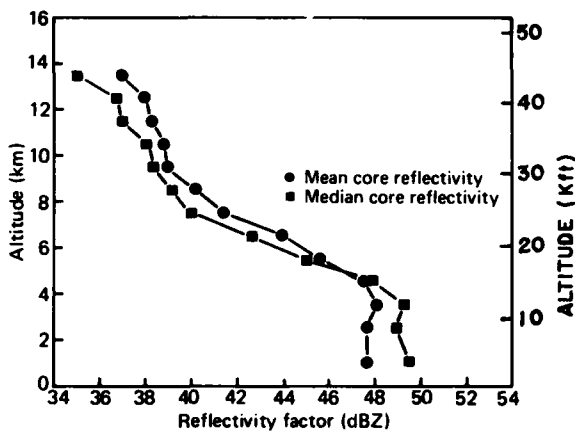


Figure 12. (Above) Profiles of mean and median reflectivity of nonsevere thunderstorms [after Konrad, 1978].

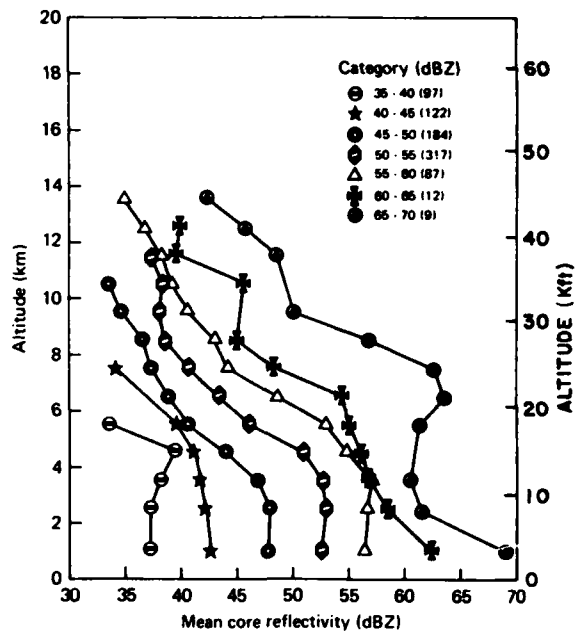
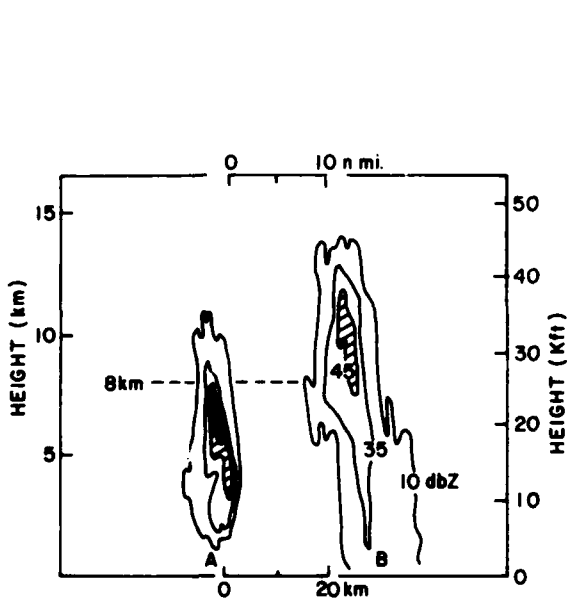
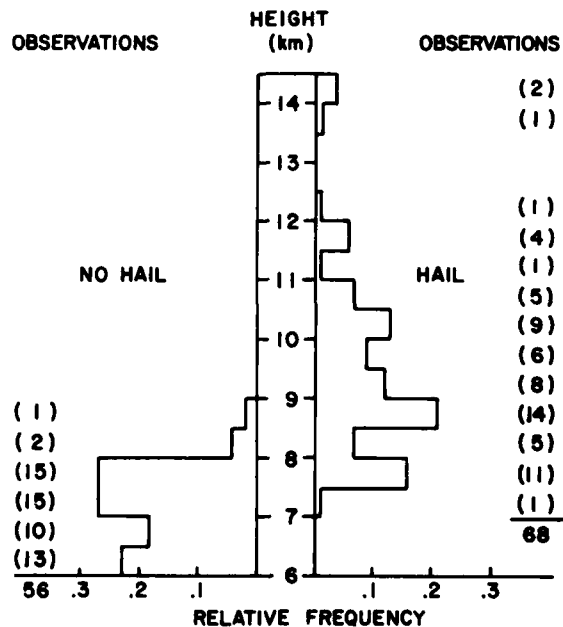


Figure 13. (Above, right) Profiles of mean core reflectivity for various categories of maximum reflectivity [after Konrad, 1978].



(a)



(b)

Figure 14. (a) Comparison of reflectivity in rain only and hail producing storms, and (b) observed heights of 45 dBZ reflectivity levels in rain only and hail producing storms.

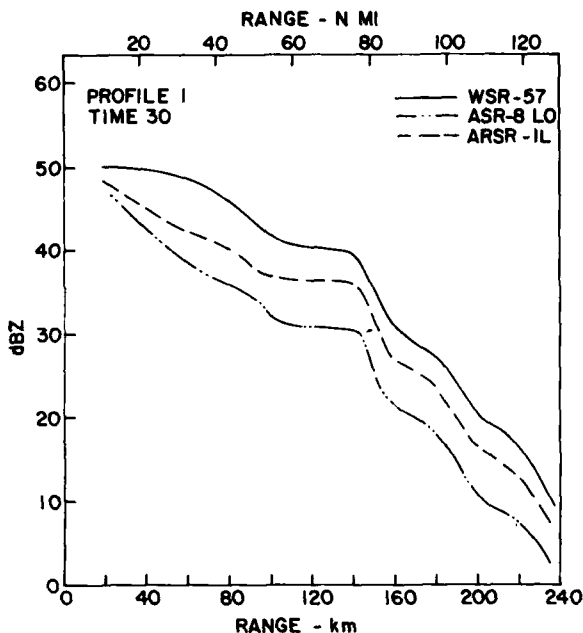


Figure 15. Reflectivity profiles which depict the performance of the WSR-57, ASR-8, and ARSR-1 radars at various ranges given model 1 storm profile at time 30 (when heavy rain has reached the ground).

Note: Maximum ASR-8 operational display range is 60 n.mi. Weather beyond 67.5 n.mi. may display ambiguously if sufficiently strong to override STC effect. Perturbations in curves are caused by stepped input storm profile data.

Core reflectivity exceeds 50 dBZ and remains a maximum at a height of 20,000 to 25,000 ft until the storm begins to dissipate.

During the 10 to 20 minutes of initial storm development, the WSR-57 radar (operating at one degree tilt or less) undershoots most of the precipitation, whose echo intensity is less than 20 dBZ. When heavy rain reaches the ground (time step 3), the WSR-57 radar measures within 5 dB of the true storm intensity at ranges between 65 n.mi. (120 km) and 110 n.mi. (204 km); and when rain and hail are heaviest at the ground (time step 4) and severe weather most likely, the WSR-57 radar measures greater than 45 dBZ at all ranges between 20 n.mi. (37 km) and 60 n.mi. (111 km).

In contrast, the ASR radars detect the storm's potential for severity (45 dBZ) one time step (3) sooner than the WSR-57. No undershoot is experienced within about 30 n.mi. Between 20 n.mi. (37 km) and 60 n.mi. (111 km) the perceived radar reflectivity varies nearly as $R^{-2.3}$.

The capability of the ARSR radar is nearly the same as the WSR-57 radar, except it detects the intensifying storm a few minutes earlier, and degrades slightly faster with range.

Models 5 and 6 - Very Severe Thunderstorms

This class of thunderstorms warrants public (and aviation) warnings because of its capability to produce large hail, tornadoes, and organized line squalls of heavy rain and damaging wind (gust fronts). Recent measurements with Doppler radars have disclosed well-organized, cyclonic circulations (mesocyclones) which accompany some of these storms and provide the intense convergence needed for large tornadoes [Burgess, Lemon, 1976].

The greatest dangers to aviation accompanying this type of storm are large hail that may be carried some distance from the storm center, and the strong gust front and associated turbulence that moves ahead of the downdraft as it spreads laterally over a distance of several miles.

The first echo that portends the development of this class of severe thunderstorm begins very high--about 25,000 to 30,000 ft (7.6-9.1 km). Since severe storm updrafts are very strong and persistent, the reflectivity increases quickly as graupel collects supercooled cloud and raindrops. Strong wind shear, frequently associated with severe storms, separates newly formed precipitation and downdraft air from the updraft, and helps establish the mesocyclone circulation. The storm's radar signature often appears as a hook echo, substantiated by Doppler radar as a rainfall pattern indicative of an organized circulation [see Burgess and Brown, 1973].

Without Doppler capability, the NWS and FAA radars cannot perceive mesocyclone beginnings, but present (as a warning) only the rapidly intensifying echo. The ASR radars detect this type of storm well--showing about 10 minutes before the WSR-57 detects the same precipitation when it reaches a much lower altitude. Beyond 67.5 n.mi. (125 km), the storms may display on the ASR ambiguously as "multiple trip" echoes when sufficiently strong to override the STC effect, and may obscure and complicate the display of any nearby storms.

On the ARSR radars, model 5 and 6 storms appear strong to a range of 130 n.mi. (241 km), which is the maximum quantitative reporting range for the NWS' WSR-57 radar.

4. SUMMARY FOR STRONG, SEVERE, AND VERY SEVERE THUNDERSTORMS

The analysis of strong, severe, and very severe thunderstorm reflectivity profiles (models 3 through 6) suggests the following conclusions:

1. The FAA ARSR radars have distinct advantage (because of their wide vertical beams) in their early detection of all severe thunderstorms that develop within 85 n.mi. (157 km); beyond that range the measured intensity decreases steadily, with a range dependency (varying with storm intensity) of $R^{-2.3}$ to $R^{-4.5}$.
2. The ASR radars are hampered by multiple trip returns whenever severe storms occur at ranges between 70 n.mi. and 140 n.mi. (130-259 km).
3. ASR radars show echoes from severe storms by displaying 40 dBZ intensity or greater during the building stage. Later, when the surface rainfall rate is at a maximum, the displayed intensity decreases. This may falsely indicate storm weakening. Severe conditions should be assumed for at least an additional 20 minutes, or until the displayed intensity falls below 25 dBZ.

4. On the ARSR radars, the displayed intensity of severe storms exceeds 40 dBZ at ranges within about 110 n.mi. (204 km). Beyond 110 n.mi. (204 km), the displayed intensity maximizes while the storm is developing and then begins to decrease at about the time when severe weather occurs at the ground. The storm should be assumed severe for about 20 minutes after the echo intensity maximizes.

5. CONCLUSIONS

FAA radars are not now optimized for detecting, measuring and displaying return from precipitation. Light rainshowers are not displayed when MTI and CP are used.

FAA radars detect the heaviest precipitation within severe thunderstorms to a range of about 130 n.mi. (241 km) for ARSR and 60 n.mi. for ASR.

The measured reflectivity on FAA and NWS radars from the heaviest precipitation within severe thunderstorms varies considerably with range and with growth cycle of the storm. (For characteristic variations with model storms analyzed, see Appendix A.)

With developing severe storms within 65 n.mi. (120 km), the FAA radars display larger and more intense echoes than the WSR-57 radar operating with no antenna tilt. When the storm is most intense, with descending tops, and heavy rain and hail (and strong winds) are likely to be occurring at ground level, the FAA radars measure somewhat less reflectivity than the NWS WSR-57 radar.

Because of seasonal and geographical variations of the heights and intensities of severe thunderstorms, the relative performance of the FAA and NWS radars varies. When the moisture content is small and the tropopause low, the storms may have relatively low tops and be seen differently by FAA and NWS radars.

The very large, intense storms known as "super storms" because of their organized flow patterns and production of large hail, tornadoes, and dangerous gust fronts, show intense echoes on FAA radars prior to severe weather better than NWS radars operating without tilt.

Again, the use of special techniques reduces the intensity of severe storm echoes (i.e., MTI, C.P.) and complicates the interpretation of the FAA radar displays. (See INTRODUCTION for possible improvements.)

Another degrading effect is the use of STC waveforms that are adjusted differently at each FAA radar facility for best aircraft detection. STC compensation for weather is, however, being incorporated into new equipments.

The higher PRF, and resulting short range of the ASR radars compromises use of this radar for severe storm surveillance because the return from severe storms is sufficient to be detected as second, and sometimes third

trip return. This may complicate the display; and coordination by telephone between controllers and forecasters may become difficult. (See INTRODUCTION for possible corrections; also see Phase 1 NSSL report by Zittel [1978] for discrimination of multiple trip weather with PRF staggering and angular shaped distortion.)

If the examples of reflectivity profiles used in this analysis are accepted as representative of most severe storms, the reflectivity levels best suited for display on the ASR radar are approximately 20 dBZ and 40 dBZ. Appearance of the first level should signal the controller to seek advice from the NWS forecaster concerning expected intensification. The appearance of the second level should be considered as a warning to the controller that severe weather (hazardous to flight) may develop within minutes and aircraft in the vicinity should be so advised. A further discussion with the ARTCC forecaster should follow as soon as possible.

Because of the influence of various air mass characteristics on storm structure, controllers should receive a briefing by a qualified forecaster concerning the type of activity expected. If echoes on the FAA radars do not agree with those expected (from the weather briefing), or indicated by the briefer as being displayed by the NWS radar, the controller should seek an explanation, or an updated advisory. In some cases, the NWS forecaster may advise controllers to consider the first level displayed as indicative of severe weather, because the precipitation echo is expected to be unusually weak, or because the development to severity is expected to be exceptionally rapid.

SUPPLEMENTARY REMARKS

There are endless variations in reflectivity profiles and associated effects on echoes displayed by air traffic control radars. Many conditions can be estimated in some detail from calculations illustrated in this report. However, that would serve no real purpose, since reflectivity details can not be elucidated in real time.

In light of inherent uncertainties, users should be cautious in their interpretations of radar measurements and should seek to match ATC radar displays to severe storm advisories received from NWS radar offices. The surveillance meteorologists now positioned at ARTCC's are faced with coordinating observations from NWS and FAA radars. This brief analysis should help prepare them for this task. There are no "magic numbers" to separate severe and non-severe thunderstorms. Sometimes the intensification is gradual, and the interpretation of severity is probabilistic. On rare occasions, growth is so rapid (less than 15 minutes) there is not time to disseminate warnings in the present advisory system. Gradually, new knowledge will be added on storm structure, which will improve criteria. The development of Doppler measurements will be a significant step forward in the direct sensing of wind and turbulence [Lee, 1977]. It will be many years before we automate the insight offered by a meteorologist who translates a variety of meteorological measurements within the framework of the air traffic control system. But we can

expect immediate improvement in the timeliness and accuracy of severe storm advisories to controllers and pilots if meteorologists are provided with modern displays of both NWS and FAA radars, and if a common language and understanding of warning criteria are agreed upon.

ACKNOWLEDGMENTS

Motivation for this research came from discussions with Mr. James Muncy, FAA, whose advice is gratefully acknowledged. The authors express their appreciation to Mr. Isadore Goldman, FAA, for his careful review and helpful comments. The color photographs of the NSSL radar were taken from the Air Force Geophysics Laboratory displays with the assistance of Mr. Doug Forsyth and Mr. Mike Kraus. Mrs. Joan Kimpel and Mr. Charles Clark, NSSL Graphic Arts Section, prepared the illustrations. Mrs. Evelyn Horwitz prepared the manuscript. Several of the illustrations were drawn from past reports and scientific papers, which provide particularly important background to this study.

REFERENCES

- Brown, R. A., 1976: The Union City, Oklahoma tornado of 24 May 1973. R. A. Brown, Ed., NOAA Tech. Memo. ERL NSSL-80, 215-228.
- Burgess, D. W., and R. A. Brown, 1973: The new structure of a severe right-moving thunderstorm: New single Doppler radar evidence. Preprints, 8th Conf. Severe Local Storms, AMS, Boston, MA, 40-43.
- Burgess, D. W., and L. R. Lemon, 1976: The Union City, Oklahoma tornado of 24 May 1973, Chapt. 5. R. A. Brown, Ed., NOAA Tech. Memo. ERL NSSL-80, 35-51.
- Carbone, R. E., D. M. Takenchi, and S. M. Howard, 1976: Some characteristics of convective showers in Texas as deduced from conventional radar and instrumented aircraft measurements. Proceedings, 17th Conf. Radar Meteor., AMS, Boston, MA, 143-150.
- David, C. L., 1976: A study of upper air parameters at the time of tornadoes. Mon. Wea. Rev., 104, 546-551.
- Dennis, A. S., C. A. Schock, and A. Koscielski, 1970: Characteristics of hailstorms of western South Dakota. J. Appl. Meteor., 9, 127-135.
- Dobson, E. B., A. Arnold, and F. L. Robison, 1978: Weather detection using fan beam radars. Proceedings, 18th Conf. Radar Meteor., AMS, Boston, MA, 413-416.
- Donaldson, R. J., 1961: Radar reflectivity profiles in thunderstorms. J. Appl. Meteor., 18, 292-305.

- Greene, D. R., and R. A. Clark, 1971: An indication of explosive development in severe storms. Preprints, 7th Conf. Severe Local Storms, AMS, Boston, MA, 97-104.
- Hamilton, P. M., 1966: Vertical profiles of total precipitation in shower situations. Q. J. R. Meteor. Soc., 92, 346-362.
- Harris, R.I., and J. C. Fankhauser, 1978: A complex convective storm system studied by multiple Doppler radar analysis. Proceedings, 18th Conf. Radar Meteor., AMS, Boston, MA, 252-259.
- JDOP Staff, 1979: Final Report on the Joint Doppler Operational Project (JDOP) 1976-78. Prepared by Staff of NSSL, ERL; WRB, AFGL; EDL, NWS; and AWS, USAF, 84.
- Johnson, D. B., and M. J. Dungey, 1978: Microphysical interpretation of radar first echoes. Proceedings, 18th Conf. Radar Meteor., AMS, Boston, MA, 117-120.
- Kessler, E., 1974: Model of precipitation and vertical air currents. Tellus, XXVI, 5, 520-542.
- Konrad, T. G., 1978: Statistical models of summer rainshowers derived from fine-scale radar observations. J. Appl. Meteor., 17, 171-188.
- Lee, J. T., 1977: Application of Doppler weather radar to turbulence measurements which affect aircraft. Report No. FAA-RD-77-145, 45.
- Marwitz, J. D., 1972: The structure and motion of severe hailstorms, Part II: Multicell storms. J. Appl. Meteor., 11, 166-179.
- Mather, G. K., D. Treddenick, and R. Parsons, 1976: An observed relationship between the height of the 45 dBZ contours in storm profiles and surface hail reports. J. Appl. Meteor., 15, 1336-1340.
- Pell, J., 1971: The use of broad-beam radar for quantitative analysis of severe storms. J. Appl. Meteor., 10, 1238-1251.
- Smith, P. L., Jr., C. G. Myers, and H. D. Orville, 1975: Bulk reflectivity factor calculations in numerical cloud models using bulk parameterization or precipitation. J. Appl. Meteor., 14, 1156-1164.
- Wilk, K. E., 1976: Evaluation of a remote weather radar display, Vol. I - Development and field tests. Report No. FAA-RD-75-60, 37.
- Wilk, K. E., J. T. Dooley and E. Kessler, 1965: ARSR-1D, ASR-4, and WSR-57 radars: A comparative study. NSSL Tech Circ. No. 1, 33.
- Zittel, W. D., 1976: Evaluation of a remote weather radar display, Vol. II - Computer applications for storm tracking and warning. Report No. FAA-RD-75-60, 114.
- Zittel, W. D., 1978: Echo interpretation of severe storms on airport surveillance radars. FAA Phase 1, Report No. FAA-RD-78-60, 58.

APPENDIX A

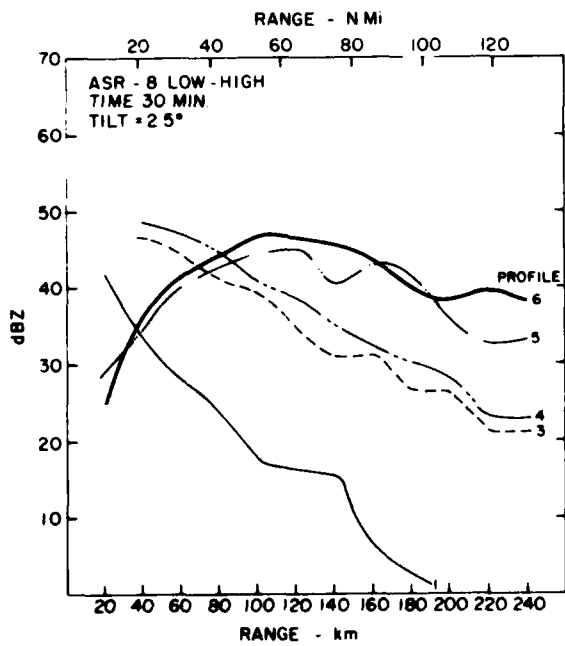
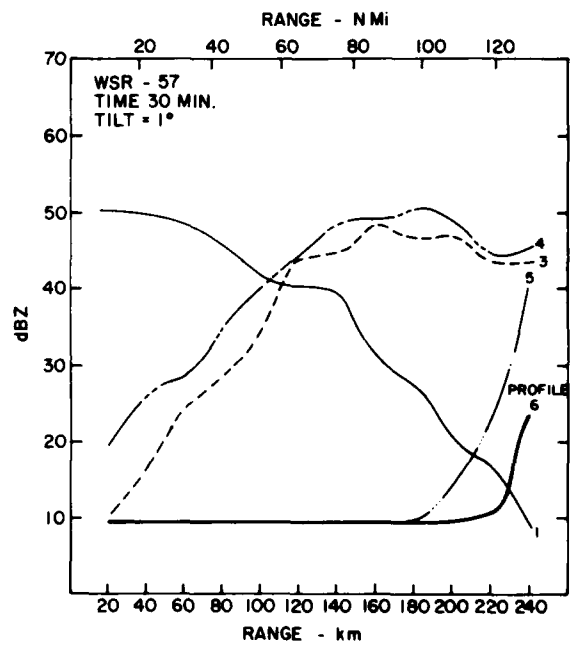
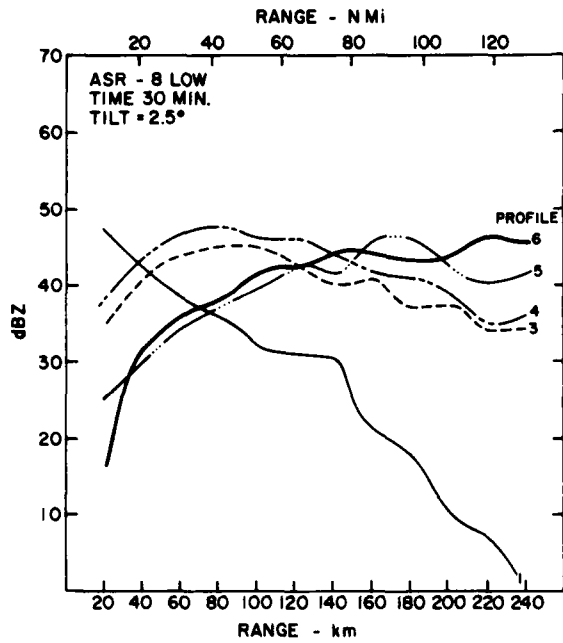
The Response of the ARSR-1L, ASR-8, and WSR-57 Radars
to Selected Storm Profiles at Specified Times and Ranges

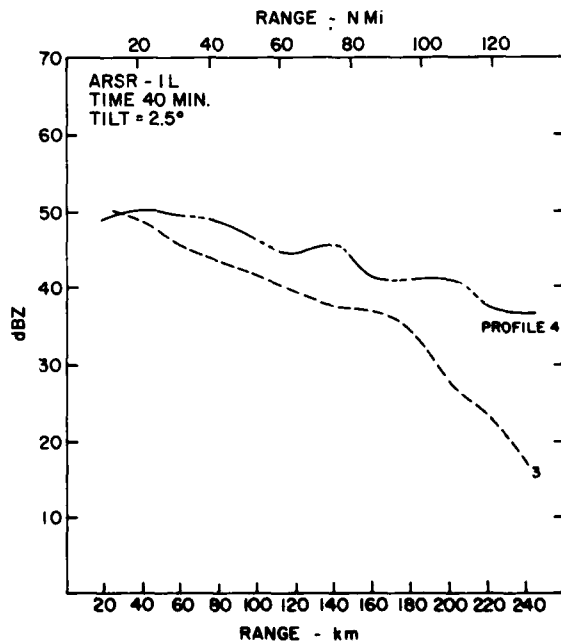
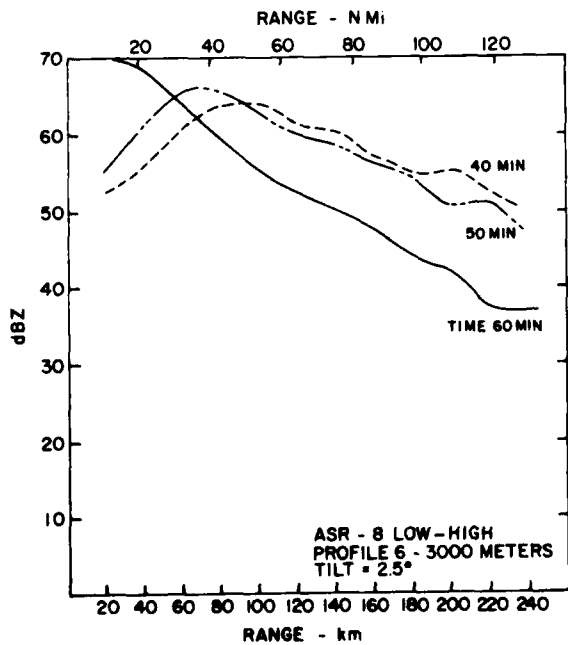
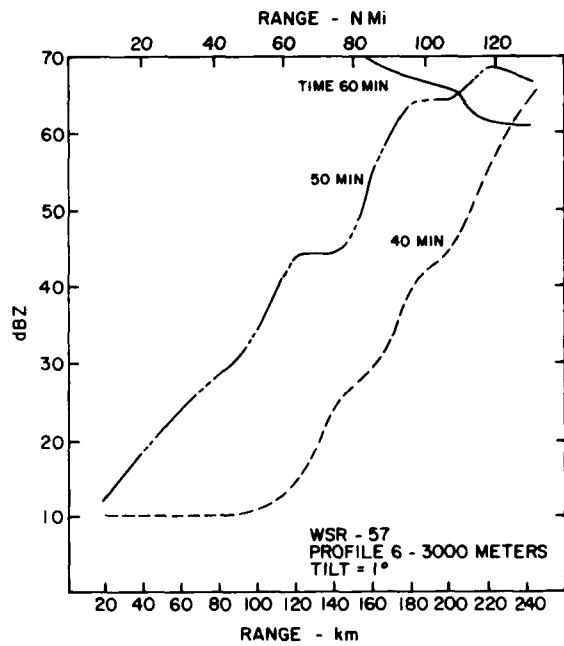
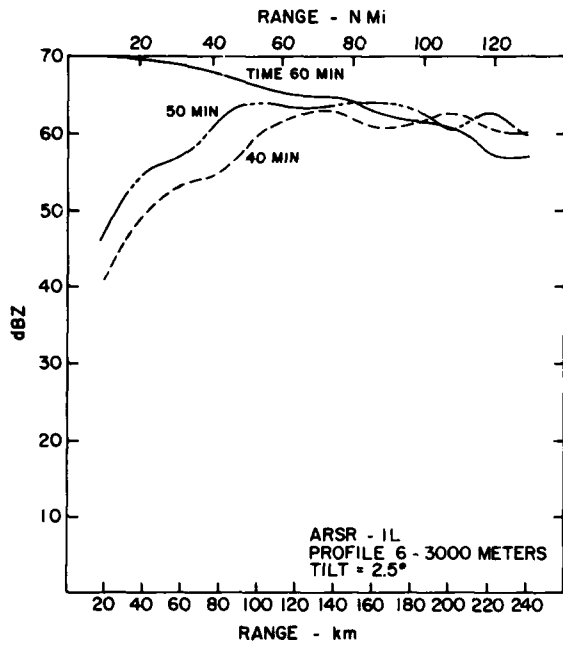
Page			
30	ASR-8 Low-High*	Profiles 1, 3, 4, 5, 6	Time 30 min.
30	ASR-8 Low**	Profiles 1, 3, 4, 5, 6	Time 30 min.
30	WSR-57	Profiles 1, 3, 4, 5, 6	Time 30 min.
31	ARSR-1L	Profile 6 - 3000 meters Cell center hgt	Times 40, 50, and 60 min.
31	ASR-8 Low-High*	Profile 6 - 3000 meters Cell center hgt	Times 40, 50, and 60 min.
31	WSR-57	Profile 6 - 3000 meters Cell center hgt	Times 40, 50, and 60 min.
31	ARSR-1L	Profiles 3, 4	Time 40 min.
32	ARSR-1L	Profiles 1, 3, 4, 5, 6	Time 30 min.
32	ASR-8 Low-High*	Profiles 3, 4	Time 40 min.
32	ASR-8 Low**	Profiles 3, 4	Time 40 min.
32	WSR-57	Profiles 3, 4	Time 40 min.
33	WSR-57, ARSR-1L	Time Profiles	R = 160 km
33	ASR-8 Low	Time Profile	R = 80 km

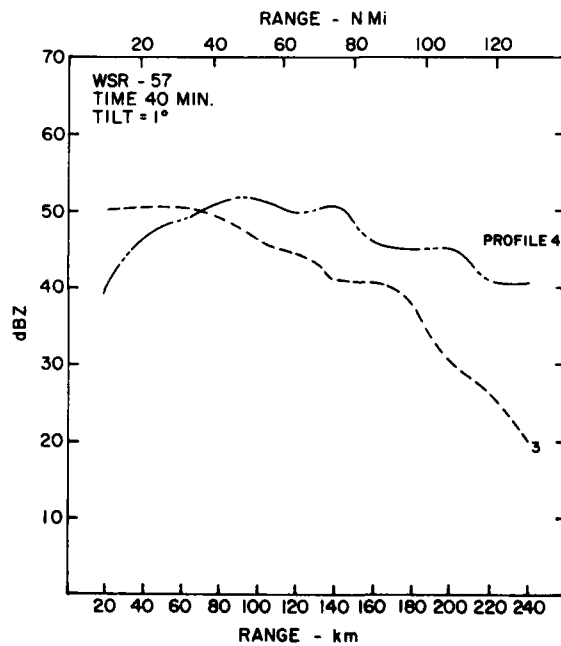
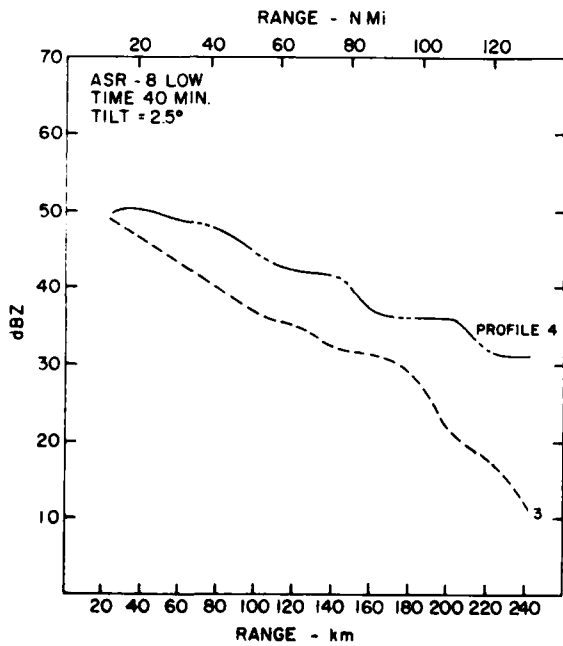
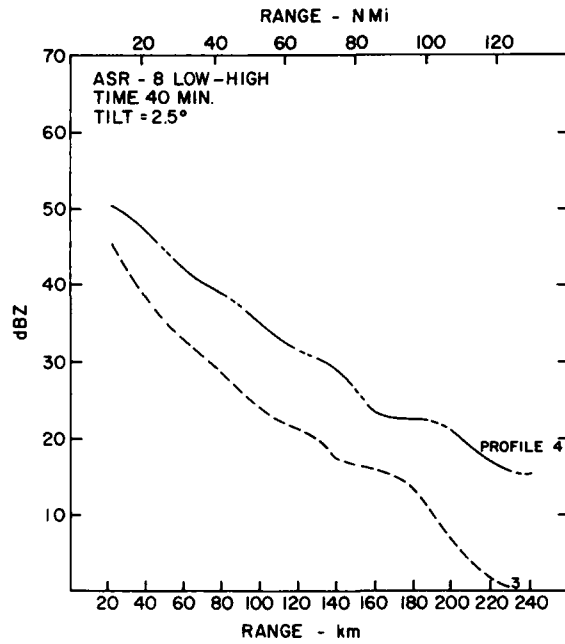
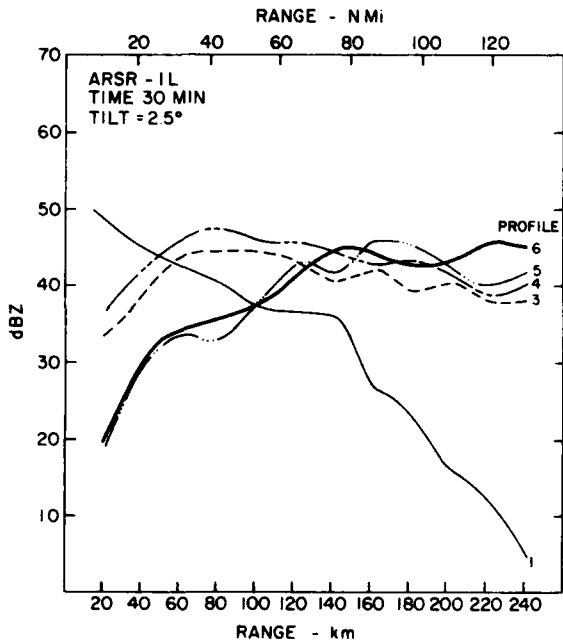
* ASR-8 Low-High transmits on low beam and receives on high beam. It is only utilized over ground clutter with range-azimuth gating (RAG).

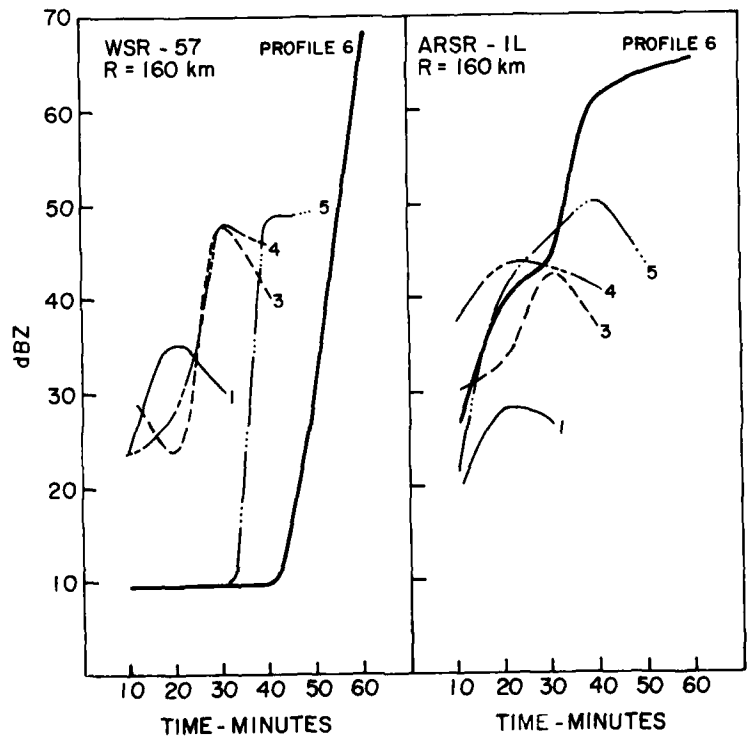
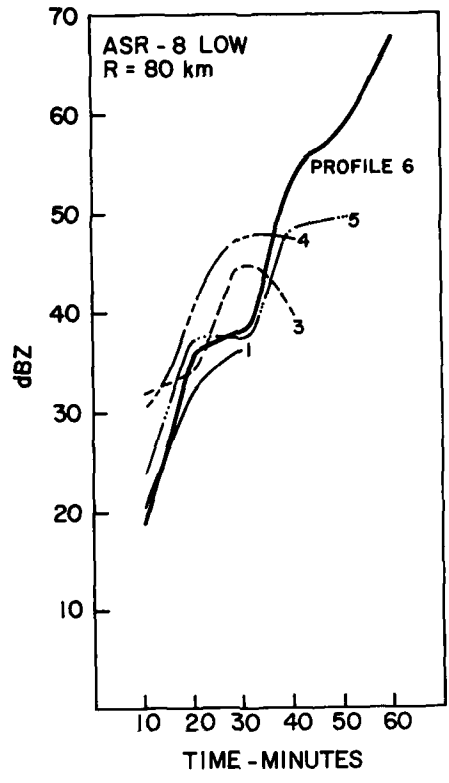
** Maximum ASR-8 operational range is 60 n.mi. Weather beyond 67.5 n.mi. may display ambiguously if sufficiently strong to override STC effect.

NOTE: Perturbations in response curves are caused by stepped input storm profile data.









APPENDIX B

Model Storm Profile Data

PROFILE 1
(dBZ vs Height for each Time Frame)

Height K ft	Time - Minutes		
	10	20	30
0.1			50
1.0			50
2.0			50
3.0			50
4.0			50
5.0			40
6.0		10	40
7.0		10	30
8.0		20	30
9.0		30	30
10.0		30	20
11.0		40	20
12.0		40	10
13.0		40	10
14.0	10	40	
15.0	10	30	
16.0	20	30	
17.0	20	30	
18.0	30	20	
19.0	30	10	
20.0	30		
21.0	20		
22.0	20		
23.0	10		
24.0	10		
25.0			

PROFILE 3
(dBZ vs Height for each Time Frame)

Height K ft	Time - Minutes			
	10	20	30	40
0.1				50
1.0			10	50
2.0			10	50
3.0			20	50
4.0			20	50
5.0			30	50
6.0			30	50
7.0			30	40
8.0			30	40
9.0			30	40
10.0			40	30
11.0			40	30
12.0		10	40	30
13.0		10	50	30
14.0		10	50	20
15.0	10	20	50	20
16.0	20	20	50	10
17.0	30	30	50	10
18.0	30	30	50	
19.0	40	30	50	
20.0	40	30	40	
21.0	40	40	40	
22.0	40	40	30	
23.0	40	40	30	
24.0	30	40	20	
25.0	30	50	10	
26.0	30	50		
27.0	20	40		
28.0	10	40		
29.0	10	30		
30.0		30		
31.0		20		
32.0		10		
33.0		10		
34.0				
35.0				

PROFILE 4
(dBZ vs Height for each Time Frame)

Height K ft	Time - Minutes			
	10	20	30	40
0.1			20	40
1.0			20	40
2.0			20	40
3.0			30	50
4.0			30	50
5.0			30	50
6.0		10	30	50
7.0		10	30	50
8.0		10	40	55
9.0		10	40	50
10.0		10	40	50
11.0		20	50	50
12.0		20	50	50
13.0		20	50	50
14.0	10	30	50	40
15.0	10	30	50	40
16.0	20	30	50	40
17.0	20	30	55	30
18.0	30	30	50	30
19.0	30	30	50	30
20.0	30	40	50	30
21.0	40	40	50	20
22.0	40	40	40	20
23.0	50	50	40	10
24.0	40	50	40	10
25.0	40	55	40	10
26.0	30	50	30	10
27.0	30	50	30	
28.0	30	50	30	
29.0	20	50	30	
30.0	20	50	20	
31.0	10	40	20	
32.0	10	40	10	
33.0		30	10	
34.0		30	10	
35.0		20		
36.0		10		
37.0				
38.0				
39.0				
40.0				

PROFILE 5
(dBZ vs Height for each Time Frame)

Height K ft	Time - Minutes				
	10	20	30	40	50
0.1					50
1.0					50
2.0					50
3.0					50
4.0				10	50
5.0				10	50
6.0				20	50
7.0				30	50
8.0				30	50
9.0				30	50
10.0				30	50
11.0				40	55
12.0				40	55
13.0				50	55
14.0				50	50
15.0				50	50
16.0				50	40
17.0				50	40
18.0				50	30
19.0			10	50	30
20.0		10	10	50	30
21.0		10	10	50	30
22.0	10	10	10	55	20
23.0	10	20	20	60	20
24.0	20	20	20	55	20
25.0	30	30	20	50	20
26.0	30	30	30	50	20
27.0	30	30	30	50	10
28.0	30	40	30	50	10
29.0	40	40	30	50	10
30.0	30	50	40	40	10
31.0	30	50	40	40	10
32.0	30	50	50	40	10
33.0	20	50	50	30	
34.0	20	50	50	30	
35.0	10	50	50	30	
36.0	10	40	50	30	
37.0		40	55	20	
38.0		30	50	20	
39.0		20	50	10	
40.0		10	40	10	
41.0		10	30	10	
42.0			30		
43.0			20		
44.0			20		
45.0			10		
46.0			10		

PROFILE 6
(dBZ vs Height for each Time Frame)

Height K ft	Time - Minutes					
	10	20	30	40	50	60
0.1						50
1.0						50
4.0						50
5.0						60
8.0					10	60
10.0					10	60
11.0					10	70
12.0					20	70
14.0					20	70
15.0					30	70
17.0					30	70
18.0				10	30	70
19.0				10	40	70
21.0				20	40	70
22.0				20	40	75
23.0				20	50	70
25.0	10			30	50	60
27.0	20	10	10	30	50	60
28.0	20	10	10	30	60	60
29.0	30	20	20	40	60	50
31.0	30	30	30	40	70	50
32.0	40	30	30	50	70	50
33.0	30	40	30	50	70	50
34.0	30	50	40	50	70	50
35.0	30	50	50	50	70	40
36.0	20	55	50	50	70	40
37.0	20	50	50	60	70	40
38.0	10	50	50	60	70	40
39.0	10	50	55	70	70	30
40.0		40	55	70	60	30
41.0		30	55	70	60	30
42.0		30	50	70	50	30
43.0		30	50	70	50	30
44.0		20	50	70	50	20
45.0		10	50	70	50	20
46.0			50	70	50	20
47.0			40	60	40	10
48.0			30	60	40	10
49.0			20	50	30	10
50.0			10	50	30	10
51.0			10	40	30	10
52.0				30	20	
53.0				30	20	
54.0				20	10	
55.0				20	10	
56.0				10	10	
57.0				10	10	